AFIT/GAE/ENY/91D-20

FAILURE CHARACTERIZATION OF A FIBER REINFORCED CERAMIC MATRIX COMPOSITE WITH CIRCULAR HOLES

THESIS

Daniel E. Bullock

Captain, USAF

AFIT/GAE/ENY/91D-20

Approved for public release; distribution unlimited

AFIT/GAE/ENY/91D-20

FAILURE CHARACTERIZATION OF A FIBER REINFORCED CERAMIC MATRIX COMPOSITE WITH CIRCULAR HOLES

THESIS

Presented to the Faculty of the School of Engineering

of the Air Force Institute of Technology

Air University

In Partial Fulfillment of the

Requirements for the Degree of

Master of Science in Aeronautical Engineering

Daniel E. Bullock, B.S.

Captain, USAF

December 1991

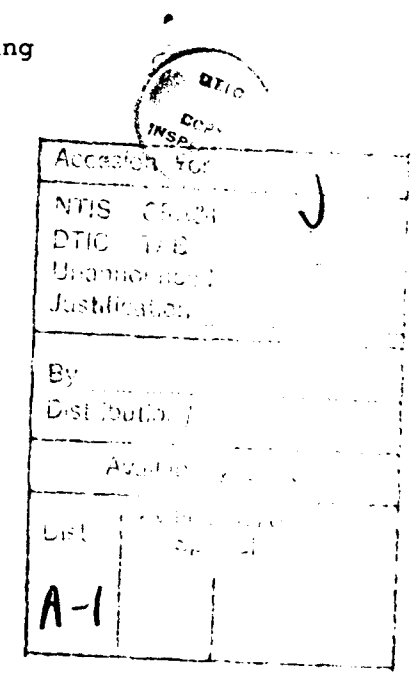

Preface

The purpose of this study was twofold: 1) to determine, for a ceramic matrix composite with a central circular hole, the relationship between failure stress and the ratio of hole diameter to specimen width; and 2) to examine how damage progresses from initiation toward failure. The ceramic matrix composite used was SiC/1723, composed of silicon carbide fibers in a glass ceramic matrix. Tensile tests were performed at room temperature on two different layups: unidirectional $[0]_8$, and $[0/90]_{2S}$ symmetric. The ultimate failure stresses were determined as the function of diameter to width ratio and compared to two current failure theories. Both non-destructive and destructive evaluation techniques were used to examine how damage initiates and progresses in the notched ceramic composites, and the stress at which initial damage occurs, as determined by strain data, acoustic emission, and replication technique, was also determined as a function of diameter to width ratio.

I would like to thank the many people in the Air Force Materials Laboratory who helped with this effort for their support, especially Capt John Pernot, Dr Tom Moran, and Mr Mark Blodgett. I would also like to thank the AFIT lab technicians who kept my equipment running; the other GAE-91D students, with whom I shared the thesis experience; and my advisor, Dr. Mall, for his assistance and patience with me. I also thank my loving wife Gaye for her understanding and encouragement, and my Lord Jesus Christ, without whom none of this would have been possible, and to whom I give all the glory.

Table of Contents

Preface ii

List of Figures iv

List of Tables vii

List of Symbols viii

Abstract x

I. Introduction 1

1. Background 2
2. Purpose 3
3. Approach 4

II. Background 6

1. Experimental Background 6
2. Theoretical Background 10

III. Experimental Procedure 23

1. Specimen Preparation 23
2. Test Equipment 29
3. Test Procedure 33

IV. Results and Discussion 36

1. Modulus of Elasticity Calculation 36
2. Data Gathering 40
3. Damage Progression and Comparison to Failure Theories . . . 44
   a. $[0]_8$ (Unidirectional) Laminate 44
   b. $[0/90]_{2S}$ (Cross-Ply) Laminate 72

V. Conclusions 93

VI. Recommendations 97

Appendix: Sample Calculations 99

Bibliography 106

Vita 109

List of Figures

Figure 1 Laminate Stacking Sequence for $[0]_8$ and $[0/90]_{2S}$ Layups .. 5

Figure 2 Principal 1-2 material axes and arbitrary x-y axes 13

Figure 3 Schematic Laminate Cross-Section 14

Figure 4 Finite Width Orthotropic Laminate With Central Circular Hole 17

Figure 5 Whitney-Nuismer Distance Parameters d_0 and a_0 20

Figure 6 Drilled Circular Hole In Specimen 25

Figure 7 Polished Inner Surface of Drilled Hole $[0/90]_{2S}$ 26

Figure 8 Specimen Configuration 28

Figure 9 Instron 4.6 kN Test Machine 30

Figure 10 22 kN Test Machine 31

Figure 11 Volume Fraction Photograph 38

Figure 12 Acoustic Emission Data Formats 42

Figure 13 Stress-Strain Curve Showing Effect of Test Pauses (90G0405B) 43

Figure 14 Matrix Cracks In Unnotched $[0]_8$ Specimen 45

Figure 15 Notched and Unnotched Cross-Sectional Area of Specimen ... 47

Figure 16 Failed $[0]_8$ Specimens 48

Figure 17 Ultimate Unnotched Area Stress as a Function of D/W Ratio . 49

Figure 18 Ultimate Notched Area Stress as a Function of D/W Ratio .. 50

Figure 19 Points of Initial Damage in $[0]_8$ Specimens 52

Figure 20 Initial Damage At Four Points in $[0]_8$ Specimen 53

Figure 21 Initial Damage At Two Points in $[0]_8$ Specimen 54

Figure 22 Failed $[0]_8$ specimen (Initial Damage at Two Points) (90G0509) 55

Figure 23 Typical Failed $[0]_8$ Specimen (90G0401) 56

Figure 24 Fracture Surface, $[0]_8$ specimen (90G0509) 57

Figure 25 Transverse Surface Cracking in $[0]_8$ Specimen 59

Figure 26 Acoustic Emission and C-Scan Before Damage in Incrementally Tested $[0]_8$ Specimen (90G0502) 60

Figure 27 Acoustic Emission and C-Scan After Damage in Incrementally Tested $[0]_8$ Specimen (90G0502) 61

Figure 28 Sectioned Specimen Showing Through Crack (90G0504) 62

Figure 29 Initial Damage Indication for $[0]_8$ Specimens 63

Figure 30 Stress-Strain Curve, Unnotched $[0]_8$ Specimen (90G0505) . . . 65

Figure 31 Stress-Strain Curve, Notched $[0]_8$ Specimen (90G0503) 66

Figure 32 Comparison of Whitney-Nuismer Point Stress Criterion to Experimental Results ($[0]_8$) 69

Figure 33 Comparison of Whitney-Nuismer Average Stress Criterion to Experimental Results ($[0]_8$) 70

Figure 34 Variation in Specimen Tab Configuration 72

Figure 35 Failed $[0/90]_{2S}$ Specimens 74

Figure 36 Ultimate Unnotched Area Stress as a Function of D/W Ratio, $[0/90]_{2S}$ 75

Figure 37 Ultimate Notched Area Stress as a Function of D/W Ratio, $[0/90]_{2S}$ 76

Figure 38 Typical Failed $[0/90]_{2S}$ Specimen (91G0203) 78

Figure 39 Fracture Surface, $[0/90]_{2S}$ Specimen (91G0210) 79

Figure 40 Acoustic Emission and Edge Replica Before Damage (91G0207) 81

Figure 41 Acoustic Emission and Edge Replica After Damage (91G0207) 82

Figure 42 Stress-Strain Curve for Unnotched $[0/90]_{2S}$ Specimen (91G0205) 83

Figure 43 Stress-Strain Curve for Notched $[0/90]_{2S}$ Specimen (91G0209) 84

Figure 44 Stress-Strain Curve Showing Second Linear Portion (91G0202) 86

Figure 45 Comparison of Whitney-Nuismer Point Stress Criterion to Experimental Results ($[0/90]_{2S}$) 88

Figure 46 Comparison of Whitney-Nuismer Average Stress Criterion to Experimental Results ($[0/90]_{2S}$) 89

Figure 47 Comparison of Ultimate Unnotched Area Stress for $[0]_8$ and $[0/90]_{2S}$ layups 91

List of Tables

Table 1 Dimensions of Test Specimens 27

Table 2 Ultimate Stresses ($[0]_8$ layup) 47

Table 3 Ultimate Stresses ($[0/90]_{2S}$ Layup) 73

List of Symbols

Symbol	Definition
a	radius of hole
a_0	Whitney-Nuismer characteristic distance for average stress criterion
A_{ij}	extensional stiffness matrix for a laminate
C	Pipes *et al.* notch sensitivity factor
d_0	Whitney-Nuismer characteristic distance for point stress criterion
D	diameter of hole
E_1	Modulus of elasticity in axial direction of composite ply
E_2	Modulus of elasticity in transverse direction of composite ply
E_x	Modulus of elasticity in load direction of composite laminate
E_y	Modulus of elasticity in direction normal to load direction of composite laminate
G_{12}	Shear modulus in the plane of the composite plate
K_T	stress concentration factor at hole (finite plate)
K_T^∞	stress concentration factor at hole (infinite plate)
m	Pipes *et al.* exponential parameter
M	magnification factor for finite width correction factor
$\{N\}$	matrix of applied force per unit width of the laminate
$[Q]$	orthotropic plane stress reduced stiffness matrix
$[\bar{Q}]$	transformed reduced stiffness matrix
R	radius of hole
$[S]$	orthotropic plane stress compliance matrix
t	thickness of a laminate
$[T]$	transformation matrix
W	width of specimen
z	distance from mid-surface of a laminate
ε	tensile strain
ε^o	mid-ply tensile strain
γ	shear strain
γ^o	mid-ply shear strain
λ	Pipes *et al.* distance parameter
ν_{12}	Poisson's ratio of compressive strain in 2 direction to tensile strain in 1 direction
σ	tensile stress

σ_x^∞	x-direction stress along y axis for infinite plate
σ_x	x-direction stress along y axis for finite plate
σ_0	ultimate stress of unnotched specimen
σ_N	ultimate stress of notched specimen based on unnotched cross-sectional area (finite plate)
σ_N^N	ultimate stress of notched specimen based on notched cross-sectional area (finite plate)
σ_N^∞	ultimate stress of notched specimen based on unnotched cross-sectional area (infinite plate)
θ	Angle between x axis and 1 axis; angle from axis normal to load direction to point of initial damage in $[0]_8$ specimens
τ	shear stress
ξ	Whitney-Nuismer distance parameter
$[0]_8$	Eight-ply laminate layup, all plies in 0° direction (0/0/0/0/0/0/0/0)
$[0/90]_{2S}$	Eight-ply symmetric laminate layup of 0° and 90° plies (0/90/0/90/90/0/90/0)

Abstract

The purpose of this study was to investigate the performance of a fiber reinforced ceramic matrix composite with circular holes. The specific objectives were to (1) determine the relationship between tensile failure stress and the ratio of hole diameter to specimen width, and (2) to examine the initiation and progression of damage. The ceramic matrix composite used was SiC/1723, composed of continuous silicon titanium carbide fibers in an aluminosilicate glass ceramic matrix. Uniaxial tensile tests were performed at room temperature on two different layups; unidirectional $[0]_8$, and $[0/90]_{2S}$ symmetric. Each layup was tested at three diameter-to-width ratios. Damage data were gathered using acoustic emission, strain gauges, replication techniques, and ultrasound (C-scan). Specimens were also sectioned after damage and examined. Strain data from the region of the hole provided the best indication of initial damage in the $[0]_8$ layup. Acoustic emission techniques accurately indicated the point of initial damage in the $[0/90]_{2S}$ layup. The Whitney-Nuismer failure theory for notched composites was adapted to allow for specimens of varying widths, and was found to fit the experimental data well.

The failure mode for the $[0]_8$ layup was longitudinal matrix splitting, initiating at the opening edge of the hole on the axis normal to the load.

Once these cracks formed, the specimen was divided into two unnotched load-bearing portions. Failure then usually occurred at the grips, which was the area of highest stress concentration. In the $[0/90]_{2S}$ layup, the failure mode was transverse matrix cracking in the 90° plies in the region of the hole at a very low tensile stress (approximately 10-20% of ultimate stress) followed by longitudinal matrix splitting on the 0° plies. Final failure was due to fiber breakage and pullout in the 0° plies along the existing transverse cracks. The failure modes for both layups followed the same pattern as in studies of graphite epoxy composites.

This material is largely notch-insensitive in the $[0]_8$ layup and entirely notch-insensitive in the $[0/90]_{2S}$ layup. For the $[0/90]_{2S}$ layup, failure stress of a specimen with a circular hole at room temperature can be accurately predicted simply by computing the notched cross-sectional area and applying the failure stress from an unnotched specimen.

Additional testing should be done on this material with holes at high temperatures. The effect of varying the load rate should also be investigated.

FAILURE CHARACTERIZATION OF A FIBER REINFORCED CERAMIC MATRIX COMPOSITE WITH CIRCULAR HOLES

I. Introduction

A composite is defined as a material composed of two or more other materials on a macroscopic scale. (This macroscopic definition distinguishes composites from alloys, for example.) Many composites have been developed as a way to obtain properties unavailable in any single material, or to achieve those properties at lower cost or weight. Examples are plywood, laminated plastics (such as Formica™), concrete reinforced with steel rods, and steel-belted tires. Even in nature, wood is a composite material, with cellulose fibers bound together in a lignin matrix. More recently, a class of advanced composites has been developed which is characterized by continuous fiber reinforced plies laminated together. One example, graphite-epoxy, is becoming well known as a material used in tennis racquets, fishing rods, etc.

1. *Background*

For advanced aerospace vehicles (as well as other purposes), materials are required that can resist high temperatures in an oxidizing environment. Ceramic matrix composites offer the potential of high fracture toughness, low density materials for these applications. Several studies have been conducted with glass ceramics reinforced with carbon fibers, but recent studies with silicon carbide (SiC) fibers show greater oxidation resistance than carbon. These glass ceramic matrix composites reinforced with SiC fibers have been shown to remain physically and chemically stable to temperatures as high as 1200° C (17). The SiC fibers also have greater stiffness than the ceramic matrices, so tensile loads are transferred to the fibers, resulting in greater tensile strength than the matrix alone can provide.

Research to date in ceramic matrix composites has concentrated on the characteristics of different combinations of fiber and matrix materials, and the failure modes of some of these composites without holes. Prewo and Brennan (4, 17) compared the performance of various glass ceramic matrix composites reinforced with SiC fibers. Marshall and Evans (14) examined the failure mode of unnotched unidirectional ceramic matrix composite specimens, and Bachmann (3) studied the failure of various unnotched cross-ply layups of SiC fiber reinforced ceramic matrix

composite. Mall and Kim (13) reported on the effectiveness of acoustic emission techniques in detecting initial damage in quasi-isotropic SiC fiber reinforced ceramic matrix composites. Also, studies have been conducted to characterize failure due to holes in graphite-epoxy composites. Tan (18) and Whitney and Nuismer (22) tested graphite-epoxy specimens with circular holes to develop failure theories for anisotropic materials, and Chang *et al.* (5) compared finite element models of graphite-epoxy composites with holes to experimental results. Ceramic matrix composite materials, however, have not been fully characterized with respect to failure due to holes.

It is important to consider the effect of holes in any design using these materials, since the majority of aerospace structures require rivet or bolt holes, access openings, instrument cutouts, or some other intentional holes in the structure. Ceramic matrix composites are different in construction and performance from metals or polymer composites; therefore, earlier hole effect findings may not be directly applicable. That need for information on hole effects is the motivation for this study.

2. Purpose

The purpose of this study was to examine the performance of a ceramic matrix composite with a circular hole under tensile load. The specific

objectives were: 1) to determine the relationship between failure stress and the ratio of hole diameter to specimen width, and 2) to systematically investigate the initiation and progression of damage.

3. Approach

The material tested is SiC/1723, a Corning 1723 glass ceramic matrix reinforced with continuous silicon titanium carbide fibers. The plies were made at the Air Force Materials Laboratory at Wright-Patterson Air Force Base and laminated into 8-ply plates, either unidirectional, $[0]_8$, or a symmetric layup of alternating 0° and 90° plies, $[0/90]_{2S}$ (Figure 1). Tests were conducted on both layups. The failure stresses and damage initiation stresses were measured for several hole diameter to specimen width (D/W) ratios, and damage progression was monitored. This was accomplished by the use of stress vs. strain data (obtained with strain gauges), acoustic emission data, C-scan (ultrasound) examination of incrementally loaded specimens, and replication techniques to examine surface cracks. Specimens were also sectioned after damage and examined.

Chapter II describes the background of this study, both the experimental research that has been done in ceramic matrix composites and the theoretical models that apply to this effort. Chapter III

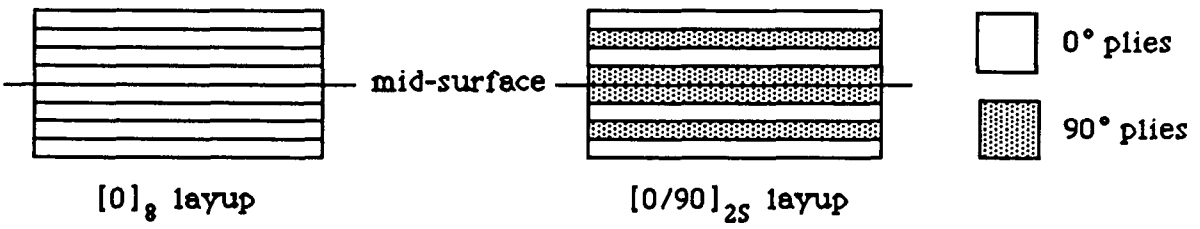

Figure 1 Laminate Stacking Sequence for $[0]_8$ and $[0/90]_{2S}$ Layups

details the experimental testing done, covering specimen preparation, test equipment, and test procedure. Chapter IV discusses the results for both layups, including calculation of elastic modulus and data gathering techniques. Chapter V presents conclusions made as a result of this study, and in Chapter VI recommendations are made regarding further testing and analysis of this material.

II. Background

1. Experimental Background

Very little work has been done with ceramic matrix composites with holes. These are new materials, and are still being characterized. Prewo and Brennan (17) performed notched-beam flexural tests on SiC/LAS (lithium aluminosilicate glass) ceramic matrix composite specimens, both unidirectional and 0°/90° cross-plied layups. They found that the SiC/LAS composite could withstand much higher loads and strain before failure than unreinforced LAS ceramic. They also found that the stress-strain curve for the composite changed slope at approximately one-half the maximum load, and considered it to be an indication of the onset of matrix micro-cracking. Brennan and Prewo (4) studied unnotched composites with matrices of Corning 7740 borosilicate glass and 7930 high-silicate glass, and concluded that the presence of discrete fibers with high strength and stiffness effectively served as a network of crack stoppers in ceramic matrix composites. Marshall and Evans (14) tested unidirectional unnotched SIC/LAS ceramic matrix composite specimens in tension and also found that the stress-strain curve became non-linear at approximately one-half of failure load. Their experiments showed that failure of this material in tension occurred in several

stages, beginning with multiple matrix cracks, followed by fiber failure and pull-out. Their analysis of crack propagation showed that once a crack reached an unbroken fiber, the stress required to extend it is independent of crack size, and they concluded that the stress required for initiation of matrix cracking is not reduced by the existence of large flaws. Since failure is initially unlocalized and occurs in the form of many small cracks instead of one large crack, linear elastic fracture mechanics (LEFM) methods based on extension of a single crack cannot be applied.

Several studies have been conducted with holes in non-ceramic composites. Tan (19) and Whitney and Nuismer (22) tested graphite-epoxy and glass-epoxy composites with circular holes and developed theories to match their empirical results; these are discussed below, under Theoretical Background. Pipes *et al.* (16) modified the Whitney-Nuismer failure theory to better match experimental data. Chang *et al.* (5) performed finite-element analysis and experimental tensile tests of various layups of graphite-epoxy composites with circular holes. They found that the notched area failure stress (load divided by minimum remaining cross-sectional area at the hole) for two different diameter-to-width (D/W) ratios was approximately equal for all layups containing 0° plies. For a $[0/90]_{6S}$ layup, their experiment indicated that damage

initiated with transverse matrix cracking in the 90° plies, starting at the opening edge of the hole on the axis normal to the load. Damage then progressed in the 0° plies as cracks in the loading direction parallel to the fibers. Final failure was due to fiber breakage in the 0° plies, occurring along the existing transverse cracks in the 90° plies. This progression of damage corresponded well to their finite element computer analysis. Tan (18) found that in $[0]_8$ unidirectional graphite-epoxy specimens with central circular holes, damage initiated with longitudinal fiber-matrix splitting at the opening edge of the hole. The splits traveled to the ends of the specimen, separating the specimen into two load-carrying portions (to either side of the hole) and a non-load-carrying portion (the pieces above and below the hole). This resulted in the specimen becoming fully notch-insensitive, since neither load-carrying portion contained a hole. This was confirmed by the notched area failure stresses, which were approximately equal for 3 D/W ratios (0.1, 0.2, and 0.3) and different plate widths (25mm, 32mm, and 46mm, all at 0.3 D/W ratio). Greszczuk's (10) study of orthotropic plates with holes showed that for both 0° and 90° orientations the maximum stress concentration occurs at the opening edge of the hole on the axis normal to the load, as is the case for isotropic materials.

Acoustic emission (AE) detection of damage initiation also has been studied. The technique has been in use in fracture analysis for many

years—Dunegan *et al.* (7) reported in 1967 that an increased acoustic count rate accompanied yielding and crack progression in metal specimens. (Counts are defined as acoustic events with an amplitude greater than a pre-set threshold, and are sometimes called events in the literature.) Awerbuch and Ghaffari (1) tested unidirectional double edge-notched graphite-epoxy specimens using a Physical Acoustics Corporation AE instrumentation system. The mode of failure of their specimens was longitudinal matrix splitting, similar to that observed in this study. They determined that initiation of this splitting was accompanied by a rapid increase in count rate. Weng *et al.* (21) reported that count rate corresponded to accumulation of damage as a result of microcracking in glass fiber reinforced liquid crystalline polyester (LCP) composites. These LCP composites are similar to glass ceramic matrix composites in that both have brittle matrices in which cracks propagate quickly. Mall and Kim (13) conducted tests on straight unnotched $[0/\pm45/90]_S$ SiC/CAS (calcium aluminosilicate) ceramic matrix composites and determined that an increase in count rate accurately indicated initial matrix microcracking well before any non-linearity was evident in the stress-strain curve.

2. *Theoretical Background*

In this study, two theoretical failure models are compared to experimental results; one by Whitney and Nuismer (22), and a modification of it by Pipes *et al.* (16). In order to apply these theories, the effective engineering constants for each laminate layup must be determined. This section first describes the procedure for calculating the laminate constants, then presents the failure models.

An orthotropic material has four basic engineering constants:

1. E_1 is the modulus of elasticity in the axial direction. This is usually the fiber direction in a fiber reinforced composite lamina.
2. E_2 is the modulus of elasticity in the transverse direction, in the plane of the lamina, and normal to the axial direction.
3. V_{12} is the Poisson's ratio for contraction in the transverse direction due to extension in the axial direction.
4. G_{12} is the shear modulus.

(The axial and transverse directions of the lamina are referred to as the principal material axes, and are denoted the 1 direction and 2 direction respectively.) For a unidirectional laminate, such as the $[0]_8$ tested in this study, these engineering constants apply directly, since the laminate acts as a single orthotropic lamina. For any layup with angled plies, however, the effective laminate constants are

different, and must be calculated as follows.

The orthotropic strain-stress relationship for a lamina in the 1-2 plane under plane stress, using the approach of Jones (11), is:

$$\begin{Bmatrix} \varepsilon_1 \\ \varepsilon_2 \\ \gamma_{12} \end{Bmatrix} = \begin{bmatrix} S_{11} & S_{12} & 0 \\ S_{12} & S_{22} & 0 \\ 0 & 0 & S_{66} \end{bmatrix} \begin{Bmatrix} \sigma_1 \\ \sigma_2 \\ \tau_{12} \end{Bmatrix} \tag{1}$$

where

ε = tensile strain in 1 or 2 direction

γ = shear strain in 12 direction

σ = tensile stress in 1 or 2 direction

τ = shear stress in 12 direction

[S] = orthotropic plane stress compliance matrix

This compliance matrix [S] can be found from the engineering constants above:

$$S = \begin{bmatrix} 1/E_1 & -\nu_{12}/E_1 & 0 \\ -\nu_{12}/E_1 & 1/E_2 & 0 \\ 0 & 0 & 1/G_{12} \end{bmatrix} \tag{2}$$

Similarly, the stress-strain relation for the same conditions

(orthotropic plane stress) is simply the inverse of Equation (1):

$$\begin{Bmatrix} \sigma_1 \\ \sigma_2 \\ \tau_{12} \end{Bmatrix} = \begin{bmatrix} Q_{11} & Q_{12} & 0 \\ Q_{12} & Q_{22} & 0 \\ 0 & 0 & Q_{66} \end{bmatrix} \begin{Bmatrix} \varepsilon_1 \\ \varepsilon_2 \\ \gamma_{12} \end{Bmatrix} \tag{3}$$

where [Q], the reduced stiffness matrix, is the inverse of [S].

These relations are defined in terms of the principal material coordinates 1 and 2. To define them in terms of an arbitrary system with principal coordinates x and y, use is made of a transformation matrix [T] defined as

$$[T] = \begin{bmatrix} \cos^2\theta & \sin^2\theta & 2\sin\theta\cos\theta \\ \sin^2\theta & \cos^2\theta & -2\sin\theta\cos\theta \\ -\sin\theta\cos\theta & \sin\theta\cos\theta & \cos^2\theta - \sin^2\theta \end{bmatrix} \tag{4}$$

where θ is the angle from the x axis to the 1 axis (Figure 2). (For the purpose of determining effective laminate engineering constants, the x-direction will be the 0° direction of the laminate.) This matrix permits transformation of the reduced stiffness matrix for use in any direction:

$$[\bar{Q}] = [T]^{-1}[Q]([T]^{-1})^T \tag{5}$$

where $[\bar{Q}]$ is the transformed reduced stiffness matrix in x-y coordinates.

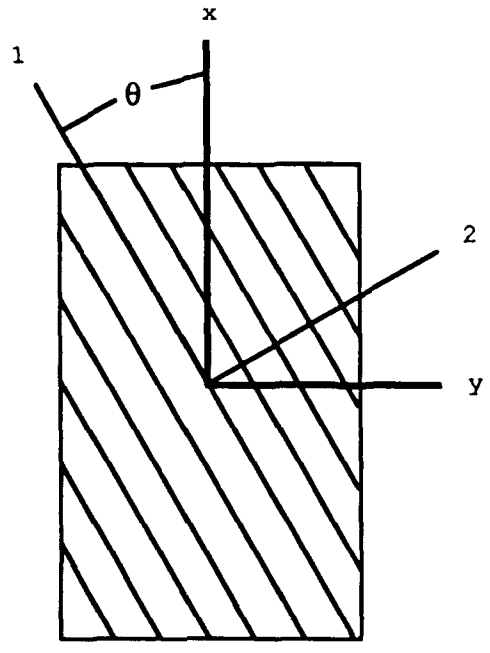

Figure 2 Principal 1-2 Material Axes and Arbitrary x-y Axes

In a laminate, the effect of each ply on the overall stiffness must be considered. Each ply is identified by number and is some distance z from the mid-surface (Figure 3). For a laminate that is symmetric about its mid-surface, the forces on the laminate can be written

$$\begin{Bmatrix} N_x \\ N_y \\ N_{xy} \end{Bmatrix} = \begin{bmatrix} A_{11} & A_{12} & A_{16} \\ A_{12} & A_{22} & A_{26} \\ A_{16} & A_{26} & A_{66} \end{bmatrix} \begin{Bmatrix} \varepsilon_x^o \\ \varepsilon_y^o \\ \gamma_{xy}^o \end{Bmatrix} \tag{6}$$

where

$$A_{ij} = \sum_{k=1}^{N} (\bar{Q}_{ij})_k (z_k - z_{k-1}) \quad \text{(extensional stiffness matrix)}$$

N_x = force per unit width of the laminate

ε_x^o = mid-ply strains

k = ply number from 1 to N

z = distance of ply from mid-surface

This procedure can be used for determining the stress-strain relationships for the $[0/90]_{2S}$ laminate used in this study. The effective tensile modulus of the $[0/90]_{2S}$ laminate can be found by noting that if only a tensile load in the x-direction is applied to a balanced (for any angle, it has the same number of plies in the positive angle direction as in the negative angle direction) and symmetric

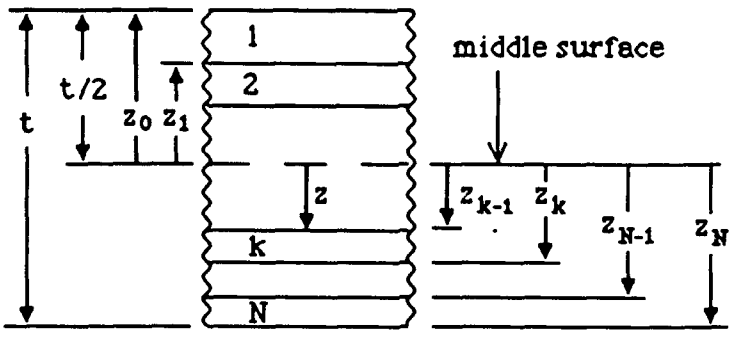

Figure 3 Schematic Laminate Cross-Section

laminate, the force-strain relation of Equation 6 becomes:

$$\begin{Bmatrix} N_x \\ 0 \\ 0 \end{Bmatrix} = \begin{bmatrix} A_{11} & A_{12} & 0 \\ A_{12} & A_{22} & 0 \\ 0 & 0 & A_{66} \end{bmatrix} \begin{Bmatrix} \varepsilon_x^o \\ \varepsilon_y^o \\ \gamma_{xy}^o \end{Bmatrix} \tag{7}$$

from which the strain in the x-direction is found to be

$$\varepsilon_x^o = \frac{A_{22} N_x}{A_{11} A_{22} - A_{12}^2} \tag{8}$$

Since, by definition,

$$\sigma_x = \frac{N_x}{t} \quad \text{and} \quad E_x = \frac{\sigma_x}{\varepsilon_x^o} \tag{9, 10}$$

where t is the thickness of the laminate, substitution results in an expression for the effective laminate modulus in the x, or 0°, direction:

$$E_x = \frac{A_{11} A_{22} - A_{12}^2}{A_{22} t} \tag{11}$$

This calculation is carried out for the $[0/90]_{2S}$ layup in the Appendix. The effective y-direction modulus can be found by the equivalent procedure in the y-direction.

To apply the desired failure theories to the results of this study, relations must be determined for stress concentration and finite width correction. Lekhnitskii (12) gives an expression for the stress concentration due to a circular hole in an infinite orthotropic plate:

$$K_T^{\infty} = 1 + \left\{ \frac{2}{A_{22}} \left[(A_{11} A_{22})^{1/2} - A_{12} + \frac{A_{11} A_{22} - A_{12}^2}{2 A_{66}} \right] \right\}^{1/2} \qquad (12)$$

where

K_T^{∞} = the stress concentration at the opening edge of the hole on the axis normal to the applied load

This stress concentration relation treats the laminate as a homogeneous orthotropic material with a single extensional stiffness matrix Aij. To find the stress concentration factor for each ply, the strain of the overall laminate at the edge of the hole must be calculated. The strain can then be used with each ply's stiffness matrix to determine ply stress concentration factors. As mentioned above, Greszczuk's (10) study of orthotropic plates with holes showed that for both 0° and 90°

lamina orientations the maximum stress concentration does occur at the opening edge of the hole.

Equation (12) above is for an infinite plate; Tan (20) gives a finite width correction factor for stress concentrations in orthotropic plates with central circular holes (Figure 4).

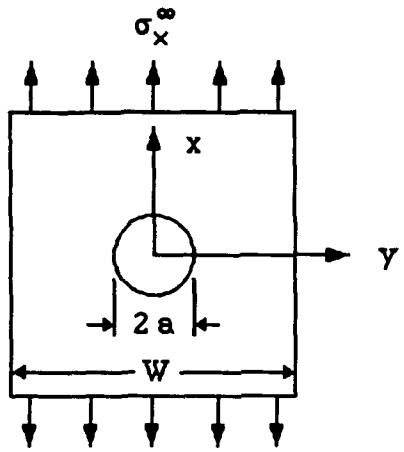

Figure 4 Finite Width Orthotropic Laminate With Central Circular Hole

(The orientation of x and y axes is chosen for consistency with the previous choice of x as the load direction.) Tan's finite width correction factor is:

$$\frac{K_T^\infty}{K_T} = \frac{3[1-(2a/W)]}{2+[1-(2a/W)]^3} + \frac{1}{2}\left(\frac{2a}{W}M\right)^6 (K_T^\infty - 3)\left[1-\left(\frac{2a}{W}M\right)^2\right] \quad (13)$$

where

K_T^∞ = stress concentration as defined in Equation (12) for infinite plate

K_T = stress concentration as defined for finite plate

and

$$M^2 = \frac{\left(1 - 8\left\{\frac{3[1 - (2a/W)]}{2 + [1 - (2a/W)]^3} - 1\right\}\right)^{1/2} - 1}{2(2a/W)^2} \tag{14}$$

Tan relates stress in a finite plate to that in an infinite plate in terms of the stress concentration:

$$\frac{K_T}{K_T^\infty}\,\sigma_x^\infty(x, 0) = \sigma_x(x, 0) \tag{15}$$

where

σ_x^∞ = x-direction stress along y axis for infinite plate

σ_x = x-direction stress along y axis for finite plate

so the finite width correction factor can be used to convert finite width stresses to the equivalent stress values in an infinite plate. Tan found that this finite width correction factor agreed well with experimental and finite element results for several layups of graphite-

epoxy composites, including 0° unidirectional and $[0/90]_S$ cross-ply symmetric.

Two failure theories for composite laminates are compared to the results of this study, one developed by Whitney and Nuismer (22), and a modification of it by Pipes *et al.* (16). Whitney and Nuismer's method for predicting the notched strength of composite laminates with circular holes assumes that failure occurs when one of the two following conditions is met: 1) either the stress at a point some constant distance, d_0, away from the hole exceeds the failure stress of the unnotched laminate (point stress criterion), or 2) the average stress over some constant distance, a_0, exceeds the failure stress of the unnotched laminate (average stress criterion) (Figure 5). These distances d_0 and a_0 are to be experimentally determined for each material (and each laminate layup), and are constants for each laminate, independent of hole radius. Thus, they are dependent both on the material and on the layup.

The point stress criterion is:

$$\frac{\sigma_N^{\infty}}{\sigma_o} = \frac{2}{2+\xi_1^2+3\xi_1^4 - (K_T^{\infty}-3)(5\xi_1^6-7\xi_1^8)} \qquad (16)$$

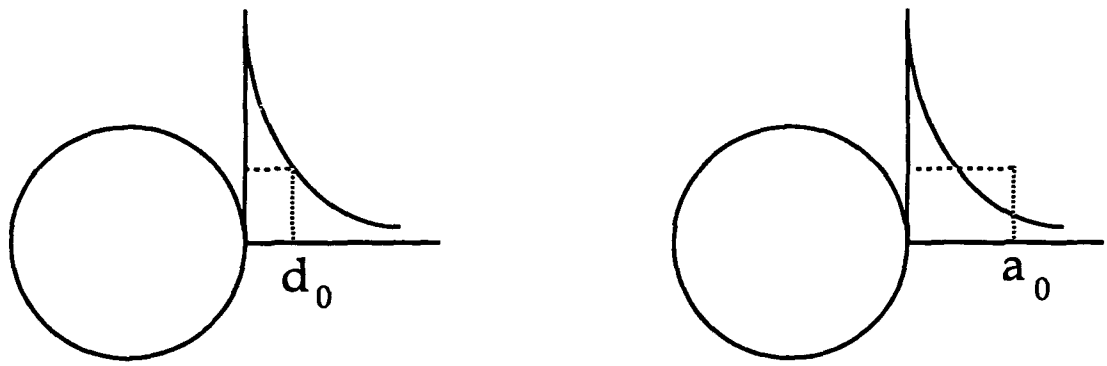

Figure 5 Whitney-Nuismer Distance Parameters d_0 and a_0

where

$$\xi_1 = \frac{R}{R + d_o} \tag{17}$$

σ_o = failure stress of unnotched laminate

σ_N^∞ = failure stress of notched laminate for infinite plate

R = radius of the hole

The average stress criterion is:

$$\frac{\sigma_N^\infty}{\sigma_o} = \frac{2(1 - \xi_2)}{2 - \xi_2^2 - \xi_2^4 + (K_T^\infty - 3)(\xi_2^6 - \xi_2^8)} \tag{18}$$

where

$$\xi_2 = \frac{R}{R + a_o} \tag{19}$$

Whitney and Nuismer found that these relations yielded good agreement with experimental results for glass-epoxy laminates with holes.

Pipes *et al.* (16) have developed a modification of the Whitney-Nuismer failure theory based on the assumption that the characteristic distance d_0 is not constant, but depends on hole radius. They assumed the relationship is exponential, i.e.

$$d_o \propto R^m \tag{20}$$

where R is the hole radius and m is the exponential parameter. Pipes *et al* then introduce a notch sensitivity parameter C and define their characteristic distance as:

$$d_o = \frac{(R/R_o)^m}{C} \tag{21}$$

where R_0 is a reference notch radius introduced to make the numerator non-dimensional. Using Whitney and Nuismer's point stress criterion, they define the ratio of notched to unnotched strength as:

$$\frac{\sigma_N^\infty}{\sigma_o} = \frac{2}{2+\lambda^2+3\lambda^4-(K_T^\infty-3)(5\lambda^6-7\lambda^8)} \tag{22}$$

where

$$\lambda = (1 + R^{m-1} R_o^{-m} C^{-1})^{-1} \tag{23}$$

Therefore, where the Whitney-Nuismer theory is a two-parameter model (σ_0 and d_0, or σ_0 and a_0), the Pipes *et al.* theory is a three-parameter model (σ_0, C, and m). C can take values from 0 to infinity; the larger its value, the more notch sensitive the material is. The exponential parameter m is bounded between 0 and 1: at m = 0, it gives the same result as the Whitney and Nuismer point stress criterion; at m = 1, the notched strength is independent of the hole radius. Pipes *et al.* point out that the theory is only applicable for $R/R_0 < 1$. If $R/R_0 > 1$, the theory would indicate notch sensitivity decreasing with increasing radius, as a result of the effect of the exponential.

III. Experimental Procedure

1. Specimen Preparation

The ceramic matrix composite material used was SiC/1723, made up of silicon carbide fibers, a binder solution, and a glass ceramic matrix. The matrix is Corning 1723 aluminosilicate amorphous glass, supplied as a ground powder, and the binder is R Hoplex liquid. The fibers are silicon titanium carbide continuous filaments manufactured by Ube Industries, Ltd., under the Tyranno Fiber brand name. They are supplied as a yarn, with a nominal mean fiber diameter of 10.5 microns. The material is formed into individual laminae with continuous unidirectional fibers, then the laminae are stacked in the desired sequence and orientation and hot-pressed to form a laminated plate. The plates provided for this study were fabricated by the Air Force Materials Laboratory at Wright-Patterson AFB. The dimensions of the plates varied: plate 91G02 was 10 cm x 10 cm; plates 90G04, 90G05, and 90G06 were 7.6 cm x 12.7 cm. (The first two digits identify the year of fabrication, and the fourth and fifth identify order of fabrication) Plate thickness varied, but was nominally 2.5 mm. Straight-edged specimens were cut from these plates with a low-speed Buehler Isomet diamond wafering saw, as described by Bachmann (3) to minimize edge

damage. For specimens with holes, the holes were drilled with a Bendix ultrasonic drilling machine, then polished on the inner surface to minimize the possibility of pre-existing stress concentrations (Figure 6). To polish the holes, brass rods were turned down to a diameter that would fit tightly in the drilled holes, then roughened slightly. These rods were used in a drill press with 25 micron lapping compound followed by 9 micron diamond suspension compound. A typical polished inner surface is shown in Figure 7. Specimens were either 6.3 cm or 10 cm long (as noted in Table 1) with phenolic polyester tabs glued on each end to minimize grip-induced damage. The tabs were 1.2 cm long for the 6.3 cm specimens, leaving a gauge length of 3.9 cm; and 2.5 cm long for the 10 cm specimens, leaving a gauge length of 5.0 cm. The configuration of specimens is illustrated in Figure 8.

The tabs were glued on with epoxy cement cured at 80°C for 1 hour. Two strain gauges were attached with cyanoacrylate glue, one at the side of the hole (on the axis normal to the load direction) and one centered 0.9 cm from the center of the hole, midway between the hole and the tab. Both were oriented longitudinally to read strain in the load direction. Strain gauges used were Measurements Group Inc. type CEA-06-032UW-120. These are small (0.81 mm long) 120-ohm gauges, with a gauge factor of 2.05. All gauges used next to the hole were of this type; occasionally

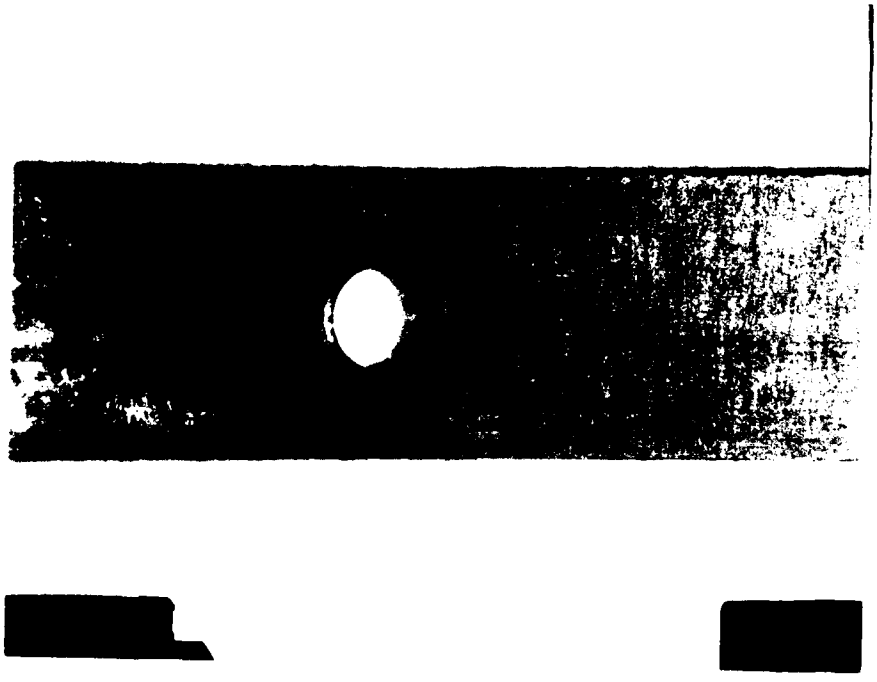

Figure 6 Drilled Circular Hole In Specimen

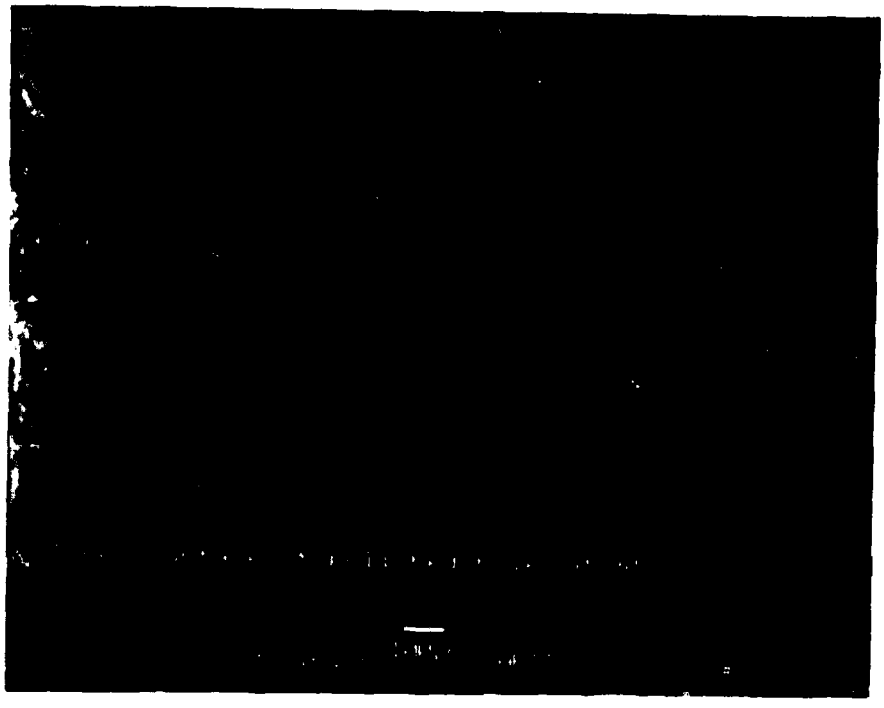

Figure 7 Polished Inner Surface of Drilled Hole $[0/90]_{2S}$

Table 1 Dimensions of Test Specimens

$[0]_8$ specimens					
Specimen	hole dia (cm)	length (cm)	width (cm)	thickness (cm)	d/w ratio
90G0401	0.136	6.35	1.255	0.262	0.109
90G0402	0.136	6.35	1.272	0.255	0.107
90G0403A	0	6.35	0.501	0.251	0.000
90G0405A	0	6.35	0.285	0.243	0.000
90G0405B	0.147	6.35	0.544	0.237	0.270
90G0408	0.190	6.35	0.477	0.226	0.398
90G0501	0.171	6.35	0.470	0.192	0.364
90G0502	0.175	6.35	0.454	0.205	0.385
90G0503	0.135	6.35	0.775	0.203	0.174
90G0504	0.175	6.35	0.688	0.211	0.254
90G0505	0	12.7	0.462	0.204	0.000
90G0508	0.191	6.35	0.764	0.214	0.249
90G0509	0.182	6.35	0.755	0.226	0.241
90G0510	0	6.35	0.521	0.217	0.000
$[0/90]_{2S}$ Specimens					
Specimen	hole dia (cm)	length (cm)	width (cm)	thickness (cm)	d/w ratio
90G0601	0	6.35	0.418	0.224	0.000
90G0602	0	6.35	0.448	0.241	0.000
90G0603	0.173	6.35	0.708	0.230	0.244
90G0605	0.145	6.35	1.200	0.232	0.120
90G0607	0.177	6.35	0.482	0.232	0.367
90G0609	0	6.35	0.406	0.224	0.000
90G0610	0	6.35	0.426	0.234	0.000
91G0201	0	10.16	0.507	0.262	0.000
91G0202	0.180	10.16	0.464	0.269	0.387
91G0203	0.143	10.16	0.543	0.275	0.264
91G0205	0	10.16	0.415	0.290	0.000
91G0206	0	10.16	0.426	0.293	0.000
91G0207	0.173	10.16	0.446	0.298	0.388
91G0208	0.147	10.16	0.531	0.301	0.276
91G0209	0.179	10.16	0.475	0.296	0.377
91G0210	0.148	10.16	1.038	0.294	0.143
91G0211	0.169	10.16	0.466	0.288	0.364

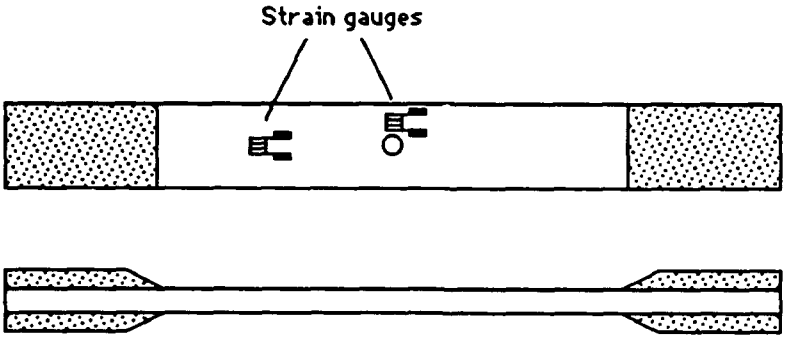

Figure 8 Specimen Configuration.

a larger gauge of the same type was used for the remote location, or on specimens without holes. Some of the plates had small amounts of curvature, resulting in variations in the linearity of stress-strain curves at low loads as the specimens straightened. They also had uneven surfaces which interfered with proper strain gauge mounting. Preparing the surface by sanding with a miniature sanding block (a 1x1x2 cm block of aluminum and 25 micron sandpaper) alleviated the surface effects and gave better strain gauge data. Specimens with no hole had only one strain gauge, mounted longitudinally at the center of the specimen.

In addition to the above specimen preparation, some of the $[0/90]_{2S}$ specimens were polished on one edge to permit crack detection by replication technique. This was done with a nylon mat on a polishing wheel, using 45 micron and 3 micron diamond paste to smooth the surface

and 0.05 micron alumina-water suspension to etch the surface to give sufficient relief for proper replication.

2. Test Equipment

Testing of the majority of $[0]_8$ specimens was done on an Instron Model 1011 material testing machine with gimballed wedge-type grips (Figure 9). The Instron is a screw-driven machine, so loading rate can only be controlled by the cross-head displacement rate. The Instron is limited to a maximum tensile load of 4.6 kilonewtons (kN); tests requiring greater load capacity were performed on one of two hydraulically driven test machines operated in load control mode; an MTS Model 810 (490 kN), and one constructed by Air Force Institute of Technology (AFIT) technicians using an MTS hydraulic actuator (22 kN) (Figure 10). The $[0/90]_{2S}$ layup testing was divided between the Instron and the 22 kN machine. The 22 kN machine could be operated in load control mode, and was equipped with grips which permitted direct control of grip pressure. During the tests, strain data was taken from the two gauges through strain gauge amplifiers and an analog-to-digital conversion card and recorded in a personal computer, using software from Instron. This software also recorded load data from the Instron test machine and calculated stress based on a user-input cross-sectional area, making possible direct plotting of load vs. strain or stress vs.

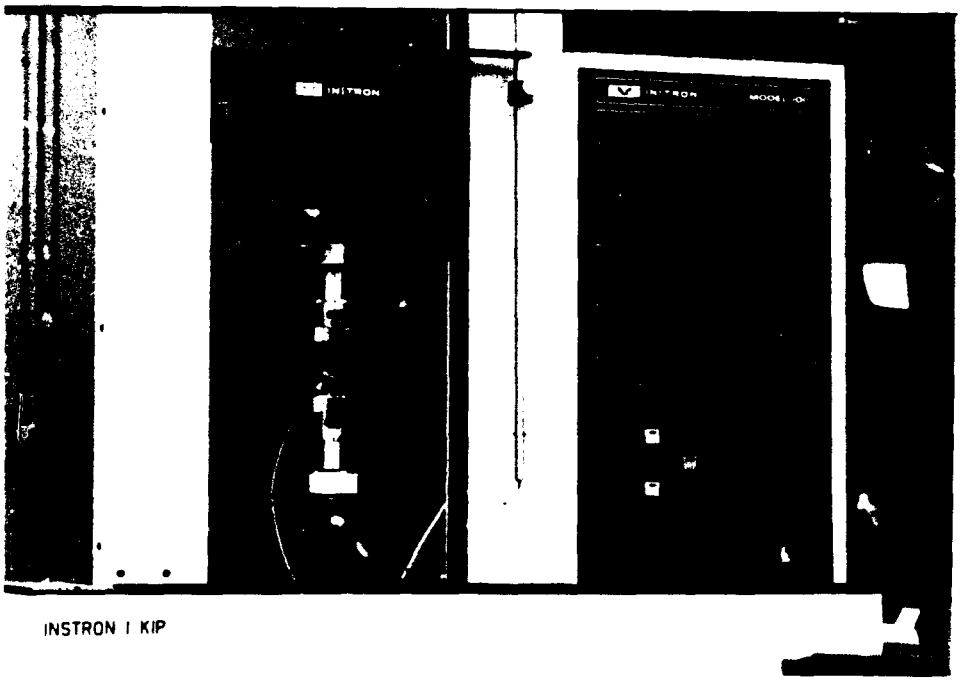

Figure 9 Instron 4.6 kN Test Machine

Figure 10 22 kN Test Machine

strain. An acoustic emission transducer was placed on each specimen, centered 1.2 cm from the hole and held against the edge of the specimen with springs or rubber bands. (When $[0/90]_{2S}$ tests were begun, it was found that the spring, if too tight, could induce failure at the point where it was in contact with the specimen.) The acoustic emission recording system was a Physical Acoustics Corporation (PAC) LOCAN AT. Acoustic output from the specimen in the 100 to 300 kilohertz range was picked up by the transducer mounted on the specimen, amplified 40dB in a PAC 1220A preamplifier, and received by the LOCAN system. The LOCAN amplified the signal again and compared it to a threshold (both the amplification and threshold are user-defined). For these tests the gain used was 30 dB and the threshold was 55 dB. These levels were determined by tests of an unnotched aluminum specimen, which would not be expected to produce acoustic output at low load levels. The gain and threshold were set to allow a small amount of acoustic activity to register (mostly machine operating noise), thus establishing a "noise floor." Any wave crossing the threshold is recorded as a "count," and is compared to pre-set attack and decay parameters to isolate individual sound-producing events, or "hits". Typically, a hit is composed of several counts, but determination of hits is dependent on prior knowledge of a material's acoustic properties, so it is unreliable for

exact quantitative analysis in a new material. For this study, plots of counts vs. load, counts vs. time (which gives count rate), and amplitude vs. load were used.

3. Test Procedure

Tests on the Instron 1011 were conducted at cross-head rates from 0.0042 to 0.013 mm/s. This can not be equated to a strain rate, however; the wedge grips allow the specimen to move relative to the grip assembly as the wedges tighten under load. Tests on the MTS systems were conducted in load control mode, at load rates of 4.4 to 8.9 Newtons per second. Acoustic emission data and strain gauge data were gathered on specimens throughout the duration of each test and saved for later analysis. The machines recorded peak loads, which were taken to be the ultimate loads of the specimens. All tests were conducted in a laboratory-air environment at room temperature (approximately 21°C).

The $[0/90]_{2S}$ layup was found to be susceptible to fracture at the grip on the Instron. It is believed that the wedge grips on the Instron machine either tightened to the point of inducing compressive failure in the specimens, or they induced bending in the specimen as they tightened. Longer tabs with small taper angles were used to reduce the pressure and stress concentration on the specimen at the tabs, as suggested by Cunningham *et al.* (6), and the tests were continued on the

22 kN machine, where there was direct control over the applied grip pressure. Results from the Instron $[0/90]_{2S}$ tests were not used for ultimate stress determination, but were used for acoustic and strain analysis.

While the test was underway, replicas were taken from the face of the $[0]_8$ and $[0/90]_{2S}$ specimens to observe damage in the area around the circumference of the hole, and, for $[0/90]_{2S}$ tests, replicas also were taken on the edge to observe damage through the thickness of the specimen (transverse matrix cracking in the 90° plies). The replicas were made with acetate film. The procedure was to apply acetone to the specimen and the film and press the film against the specimen. The acetone softened the film, which would form to the surface contour of the specimen. After a few seconds, the film set into an exact replica of the surface, and was removed. The replicas were then examined under an optical microscope.

In order to observe the progression of damage, two specimens of each layup having different D/W ratios were incrementally loaded and examined after each increment by C-scan procedure. C-scan is an non-destructive ultrasound process by which a test article can be examined at various depths by utilizing the time delay of the emitted and reflected signal. These C-scan images were correlated to strain and acoustic data for the

specimens.

Some SiC/1723 specimens were treated with dye penetrant and X-rays were taken. No damage was visible in the X-rays, even when cracks were visible on the surface of the material. It is believed that the density of the ceramic material is too close to that of the dye penetrant for cracks to be visible, or the cracks themselves are too small for the resolution of the X-ray images. Additional complications with X-ray examination were diffraction near the hole (due to the small size of the specimens) and the shadowing effect of metal strain gauges glued to the surface.

IV. Results and Discussion

This chapter discusses the experimental results and compares them to theoretical models. The first section of this chapter discusses how the nominal moduli of elasticity for each laminate layup were computed for use in the failure theories, using values provided by the Air Force Materials Laboratory for the fibers and the matrix. The second section discusses how the various data (ultimate load, acoustic emission data, acetate replicas, ultrasound, stress-strain data) were gathered during specimen testing. The third and fourth sections addresses results obtained for the $[0]_8$ and $[0/90]_{2S}$ layups, respectively, including comparison to theory.

1. Modulus of Elasticity Calculation

Jones (11) gives the following expressions (known as the *rule of mixtures*) for theoretically determining the moduli of elasticity of a composite lamina from the moduli of its constituent parts:

$$E_1 = E_f V_f + E_m V_m \tag{24}$$

and

$$E_2 = \frac{E_f E_m}{V_m E_f + V_f E_m} \tag{25}$$

where

E_1 = modulus of elasticity of the composite lamina in the axial (fiber) direction

E_2 = modulus of elasticity of the composite lamina in the transverse direction

E_f = modulus of elasticity of the fibers

E_m = modulus of elasticity of the matrix

V_f = volume fraction of the composite composed of fibers

V_m = volume fraction of the composite composed of matrix

To find the volume fractions, a specimen of the SiC/1723 composite was cut, an edge was polished, and optical micro-photographs were made (Figure 11). An average fiber diameter was determined and the fibers were counted in each photograph. The fiber volume fraction (V_f) was calculated for each photograph using the following formula:

$$V_f = \frac{n A_f}{A_p} \tag{26}$$

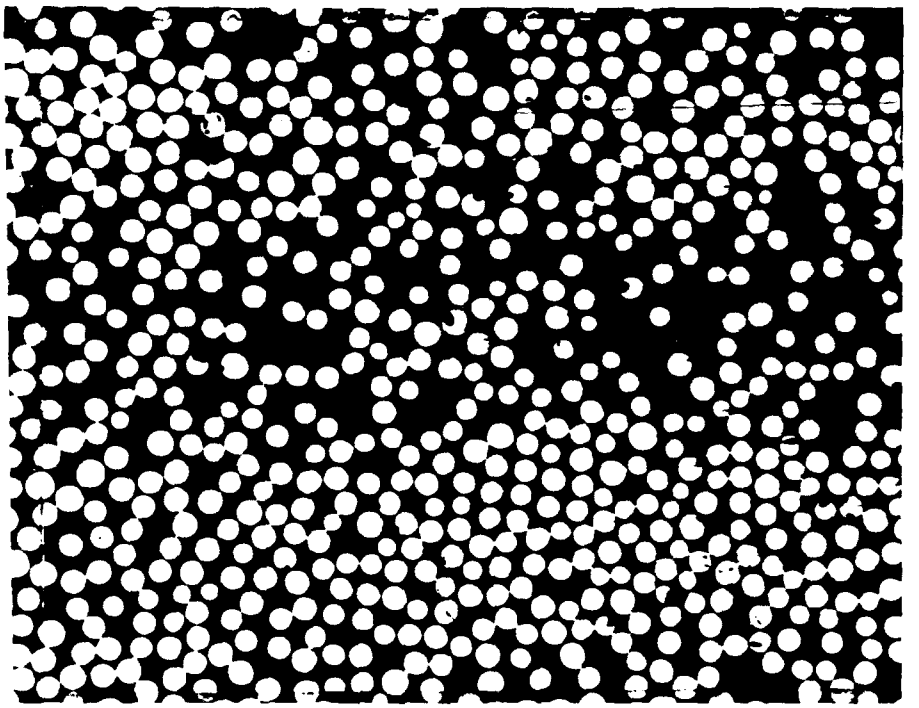

Figure 11 Volume Fraction Photograph

where n is the number of fibers, A_f is the average fiber area, and A_p is the area of the photograph. The values of V_f for each photograph were averaged to compute a nominal V_f for the composite, which was found to be 0.45. The matrix volume fraction is found by:

$$V_m = (1 - V_f) \tag{27}$$

which is 0.55 for this composite.

Zawada (23) of the Air Force Materials Lab provided the following material properties for the SiC/1723 composite used in this study.

$$E_f = 164 \text{ GPa}$$

$$E_m = 60.6 \text{ GPa}$$

These values were obtained from the manufacturers of the materials. E_f has a tolerance of ±4%; the tolerance for E_m was not determined. Using these values and Equations (24) and (25), the engineering constants E_1 and E_2 for a lamina were found to be

$$E_1 = 107.1 \text{ GPa}$$

$$E_2 = 84.6 \text{ GPa}$$

The Poisson's ratio, ν_{12} , given for the lamina was 0.18. From these constants the shear modulus G_{12} can be calculated using the relation

$$G_{12} = \frac{E_1}{2(1 + \nu_{12})} \tag{28}$$

which gives a value of shear modulus for the lamina of 45.4 GPa. These values were used directly as the moduli for the $[0]_8$ layup, since a unidirectional laminate acts as a single lamina. They also were used to produce the compliance matrix [S] in Equation (2), which in turn was used to develop the extensional stiffness matrices A_{ij} for both the $[0]_8$ and $[0/90]_{2S}$ layups, following the procedure set forth in Equations (2) through (6). These A_{ij} matrices were used for both theoretical models. For the $[0/90]_{2S}$ layup, the A_{ij} matrix also was used to solve Equation (11) for the effective laminate axial elastic modulus, E_x, which was found to be 95.9 GPa. The theoretical engineering constants are compared to experimental values later in this chapter.

2. Data Gathering

Specimens from both layups were tested at steadily increasing static load directly to failure. Load was recorded once a second, and ultimate

load was defined as maximum load sustained by the material before failure. (Failure was defined as complete separation of upper and lower portions of the specimen.) Acoustic emission (AE) data were gathered throughout the duration of the tests. The threshold was set to allow a small amount of noise to reach the system, to assure that any significant activity was not filtered out. The AE data were displayed in the following formats: load vs. time; amplitude vs. load; counts vs. time; and counts vs. load (Figure 12). Replicas were made of specimens of each D/W ratio at intervals of 220 to 450 N; these replicas were made of the hole region on both layups, and, for $[0/90]_{2S}$ specimens, the edge of the specimen. This made it possible to determine at what load damage had first appeared, and allowed correlation with the acoustic emission data. The tests were paused while replicas were taken, then resumed. Due to the design of the Instron test machine, the load tended to decrease slowly during the pauses. The effect of this pause can be seen in the stress-strain curves. At low loads, the material is still linearly elastic, and the curve re-traces itself as stress decreases. At higher loads, damage is occurring, and the strain returns along a new curve as stress decreases (Figure 13).

Also, an unnotched test specimen of the $[0]_8$ layup was polished on one side and loaded while recording acoustic emission. The intent was to show a correlation between an acoustic event and the initial

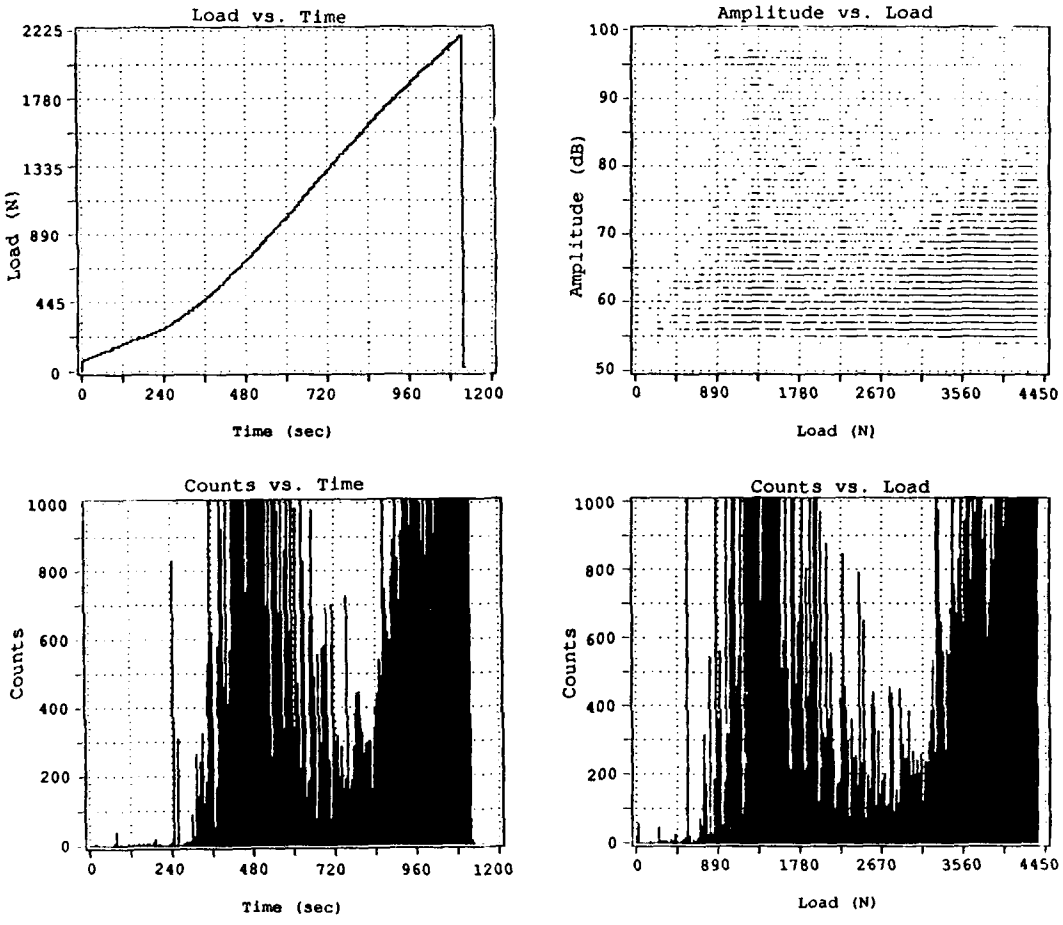

Figure 12 Acoustic Emission Data Formats

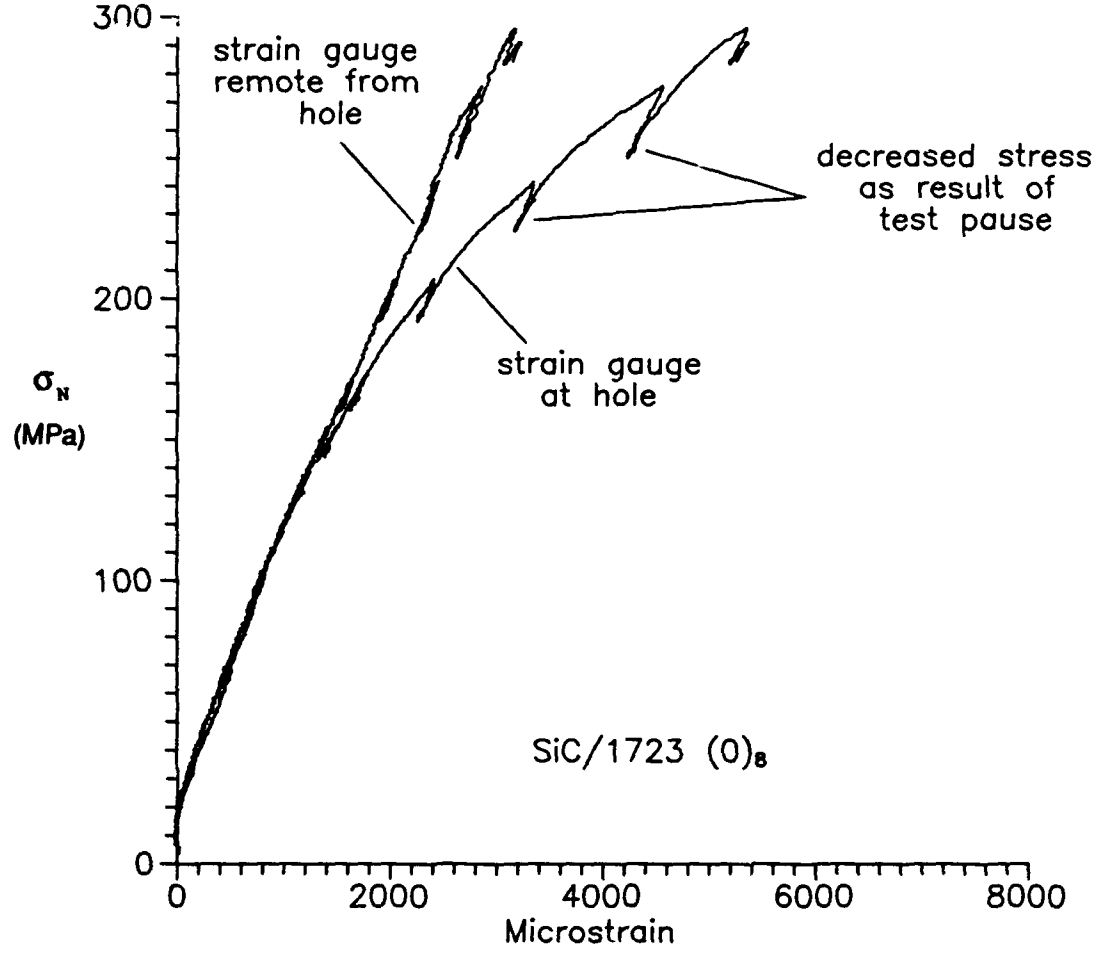

Figure 13 Stress-Strain Curve Showing Effect of Test Pauses (90G0405B)

appearance of matrix cracks on the edge of the specimen (as shown by replicas). This test was inconclusive; a high level of acoustic activity preceded the appearance of damage at the edge, and no specific acoustic event accompanied the first appearance of cracks (Figure 14). It is believed that the acoustic emission activity indicated damage that was not yet visible on the surface. Mall and Kim (13) showed that AE activity corresponded with the appearance of surface microcracking in a similar ceramic matrix composite material. Several specimens were also C-scanned; these were loaded incrementally, and removed from the machine for the C-scan procedure. This revealed defects below the surface, and was correlated with the replicas and acoustic emission. Strain gauge data were recorded with load at one-second intervals, and stress was plotted as a function of strain. These curves were examined for non-linearities which would indicate inelastic behavior, and compared to the other data.

3. Damage Progression and Comparison to Failure Theories

a. $[0]_8$ (Unidirectional) Laminate

Nine specimens of the $[0]_8$ layup were successfully tested to failure (some specimens broke prematurely at the grips instead of at the hole,

Figure 14 Matrix Cracks In Unnotched $[0]_8$ Specimen

but were not used for this analysis). The ultimate unnotched area and notched area stresses are shown in Table 2. (Ultimate unnotched area stress σ_N is defined as ultimate load divided by specimen unnotched cross-sectional area; ultimate notched area stress σ_N^N is ultimate load divided by minimum remaining cross-sectional area at the hole; see Figure 15.) The failed specimens are illustrated in Figure 16. The ultimate unnotched area stresses are plotted as a function of D/W ratio in Figure 17, and the ultimate notched area stresses as a function of D/W ratio in Figure 18. The dashed straight line in Figure 17 and in Figure 18 is the line of net strength, along which stress on the notched cross-sectional area is constant. The ultimate stress for each specimen is normalized by dividing it by the average value of all unnotched specimens from the same plate. This allows test results from different plates to be compared directly by equalizing the no-hole strengths of each plate, which were found to vary between the two plates. This method results in some unnotched specimens having ultimate stress values not equal to one, since they are normalized against the average unnotched value for their plate. Unnotched specimens from Plate 90G04 had an average ultimate stress of 510 MPa, while the value for plate 90G05 was 441 MPa.

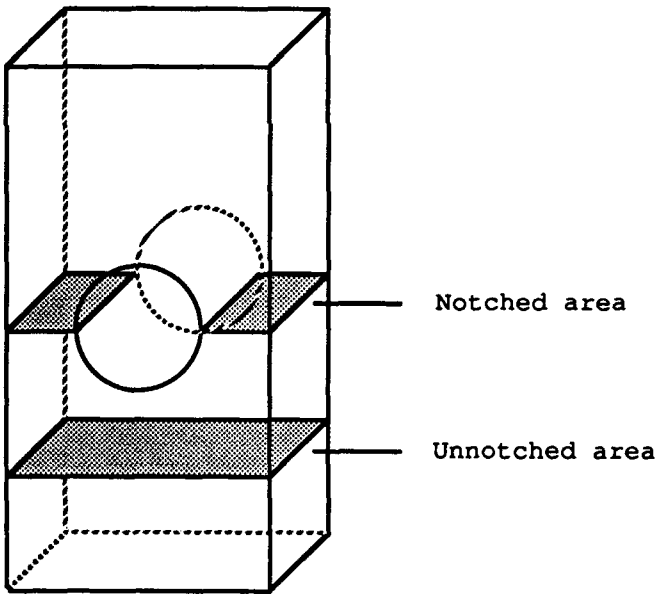

Figure 15 Notched and Unnotched Cross-Sectional Area of Specimen

Table 2 Ultimate Stresses ($[0]_8$ layup)

Specimen Number	Diameter-to-Width Ratio	Ultimate Unnotched Area Stress σ_N (MPa)	Ultimate Notched Area Stress σ_N^N (MPa)
90G0403A	0	550.2	550.2
90G0405A	0	469.7	469.7
90G0505	0	441.2	441.2
90G0401	0.109	394.1	442.0
90G0503	0.173	308.3	373.1
90G0509	0.241	406.0	535.0
90G0405B	0.270	342.0	468.4
90G0501	0.364	220.1	345.9
90G0408	0.397	288.6	479.1

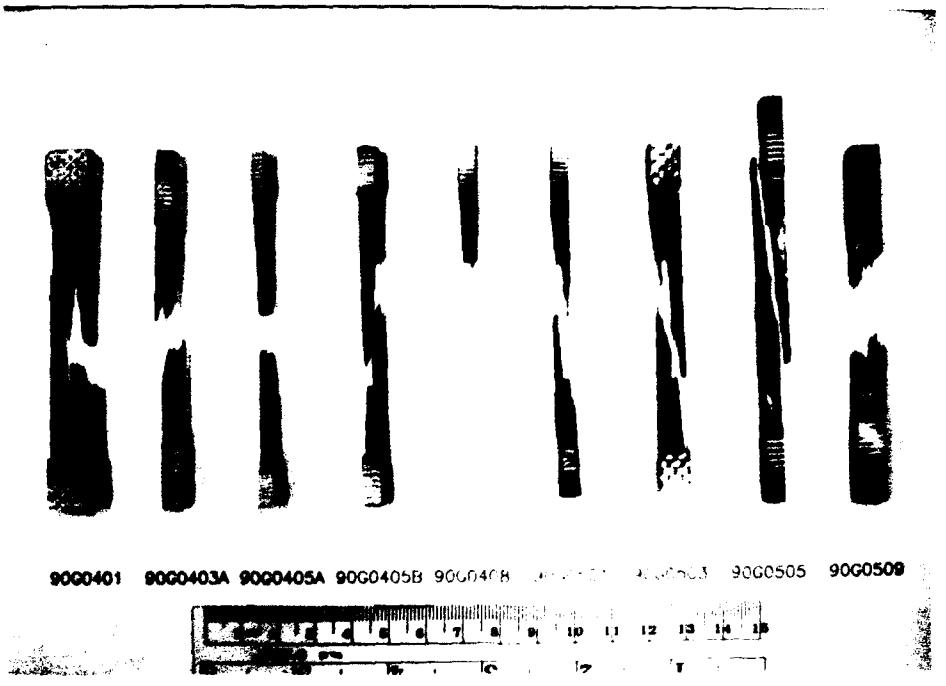

Figure 16 Failed $[0]_8$ Specimens

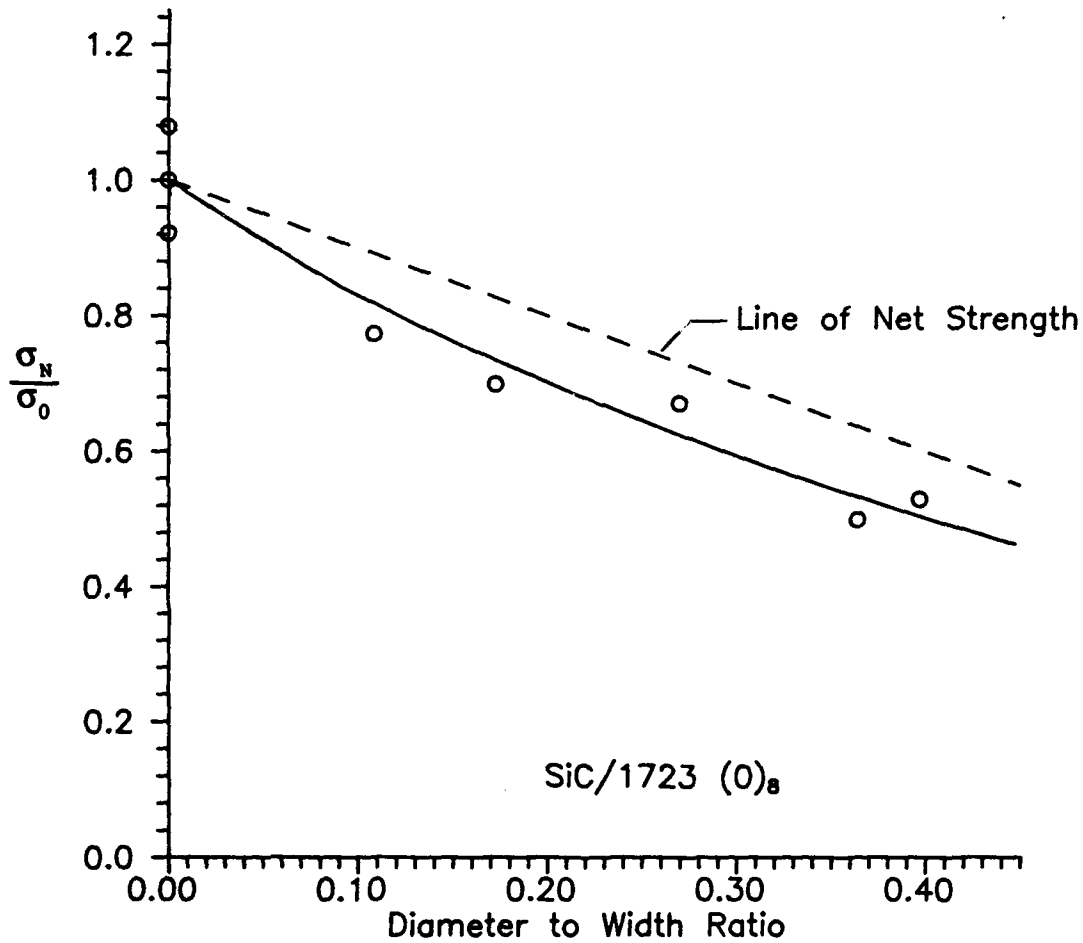

Figure 17 Ultimate Unnotched Area Stress as a Function of D/W Ratio

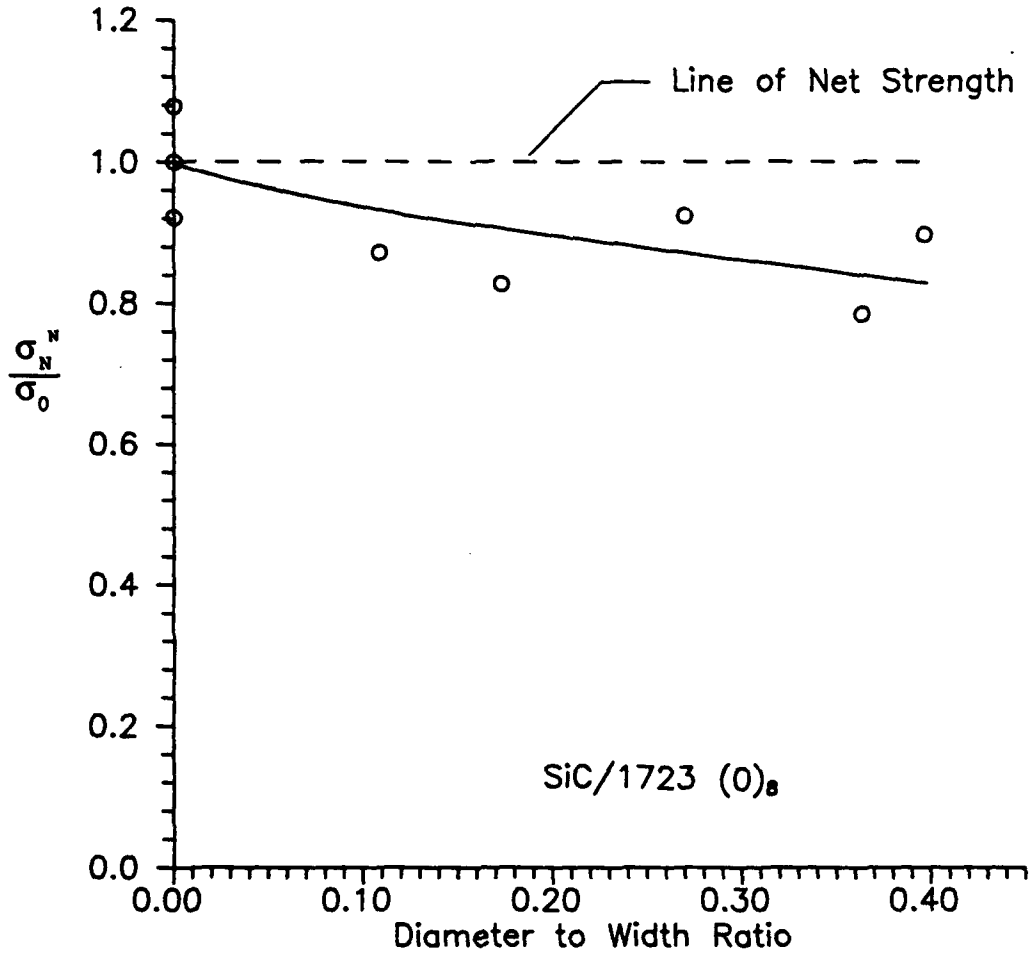

Figure 18 Ultimate Notched Area Stress as a Function of D/W Ratio

The ultimate notched stresses do not exhibit a rapid decline from specimens with no hole to specimens with holes, as would be expected in an isotropic material (due to the stress concentration induced by the hole). This indicates a high degree of notch-insensitivity. The stresses do, however, drop below the line of net strength. At the maximum D/W ratio of 0.4, the ultimate stress along the best-fit curve is 84% of the value on the line of net strength. Since the net strength line equates to the average no-hole ultimate stress applied to the notched cross-sectional area, this can be interpreted as a 16% notch sensitivity at D/W = 0.4. By comparison, Tan's (18) tests on $[0]_8$ graphite-epoxy showed no variation from the line of net strength, which he considered an indication that the material was fully notch insensitive.

The failure pattern of these specimens was matrix splits initiating at points on the hole with some angle θ from the axis normal to the load (labeled A, B, C, and D in Figure 19). The cracks radiated outward from the hole for a small distance, then progressed longitudinally to the end of the specimen. The path of the longitudinal cracks usually followed the longitudinal line through the opening edge of the hole (dotted line in Figure 19). The average value for the angle θ was determined from replicas of the $[0]_8$ specimens to be 18°, though the

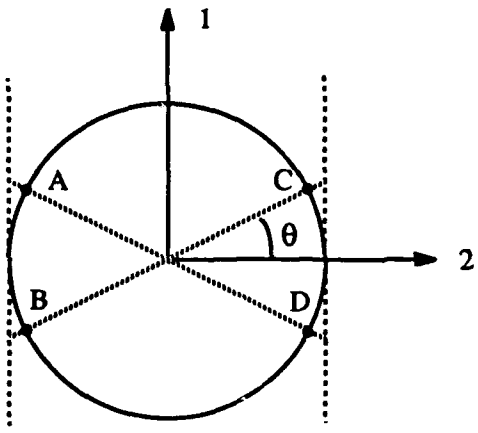

Figure 19 Points of Initial Damage in $[0]_8$ Specimens

angles varied from 5° to 25°. This splitting began well before failure (approximately 50% of ultimate load). Two different modes of crack progression were observed in the replicas. The first was cracks propagating simultaneously from all four points A, B, C, and D, as shown in Figure 20. The second was cracks propagating at two opposite points, such as A and D, as shown in Figure 21. This second mode resulted in failures such as that in Figure 22. Upon reaching the tabs the cracks grew transversely across the tab and sometimes traveled longitudinally to the other end (Figure 23). This final crack progression occurred suddenly at the point of failure. Examination of the fracture surface revealed a large amount of fiber pullout and significant matrix microcracking at failure (Figure 24). It also was observed tnat the

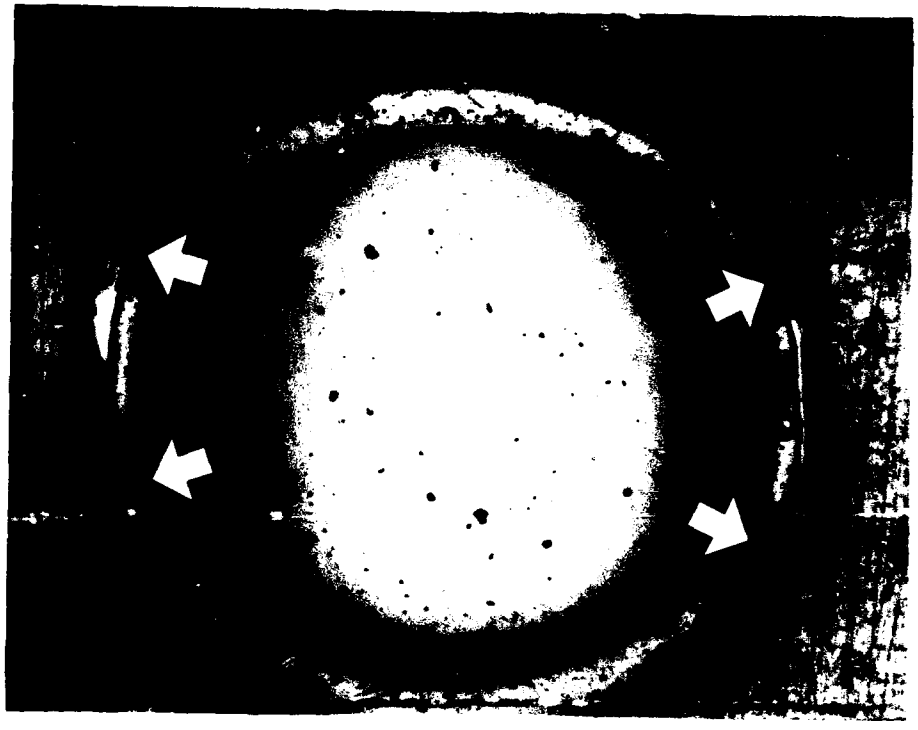

Figure 20 Initial Damage At Four Points in $[0]_8$ Specimen

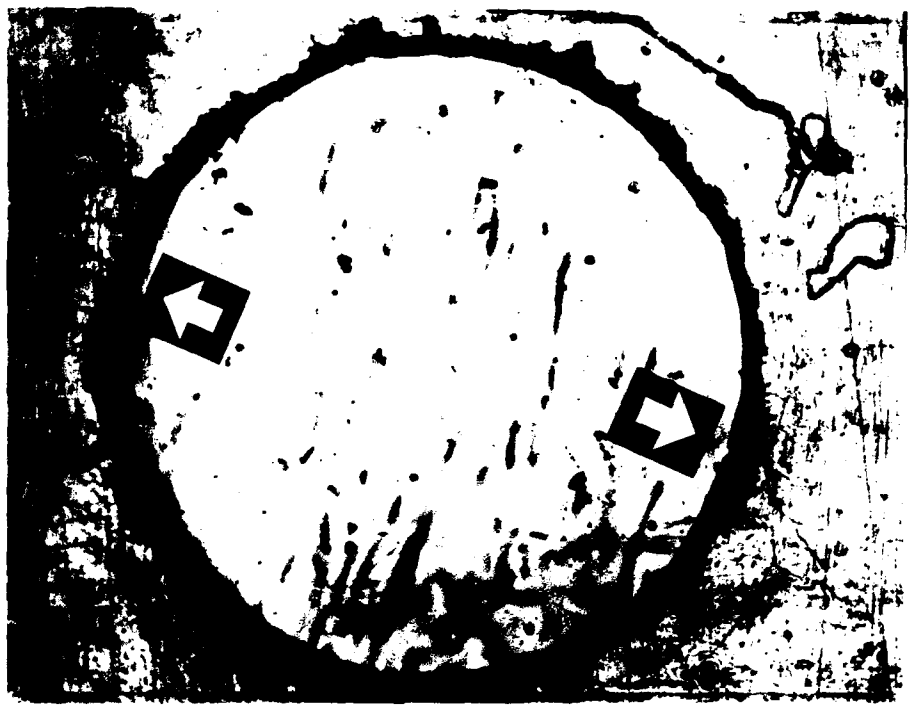

Figure 21 Initial Damage At Two Points in $[0]_8$ Specimen

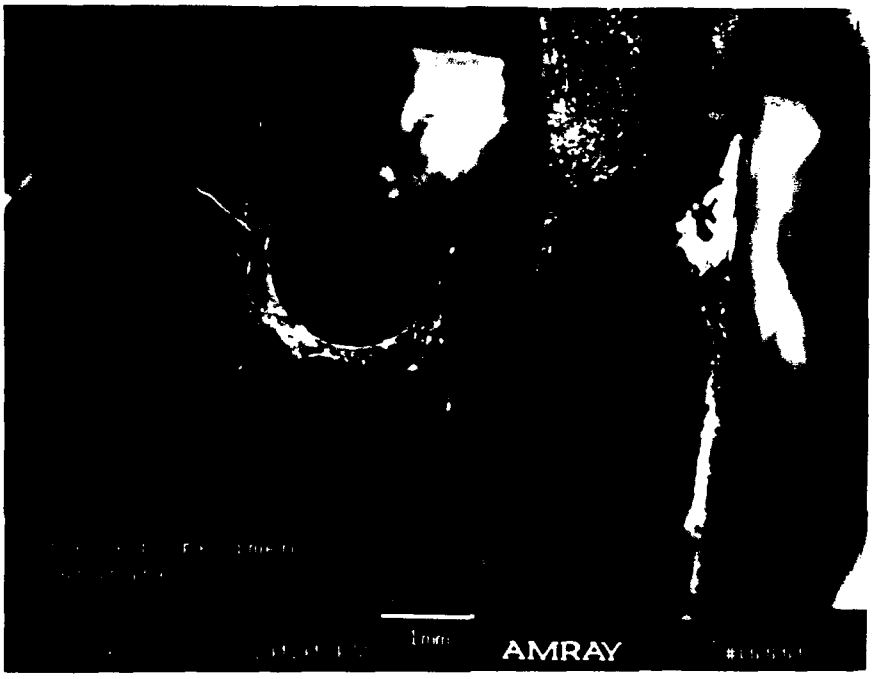

Figure 22 Failed $[0]_8$ specimen (Initial Damage at Two Points)

(90G0509)

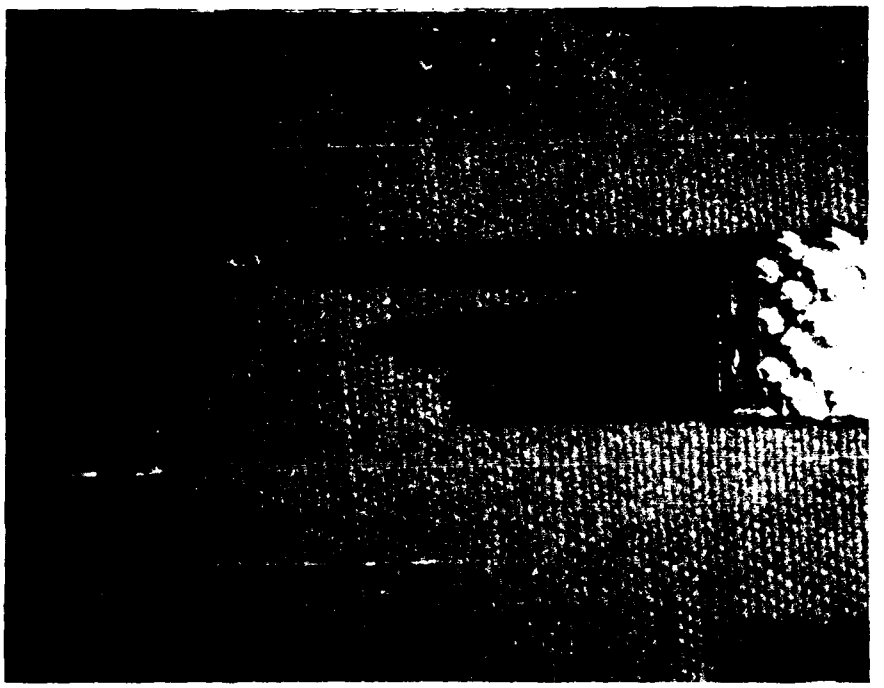

Figure 23 Typical Failed $[0]_8$ Specimen (90G0401)

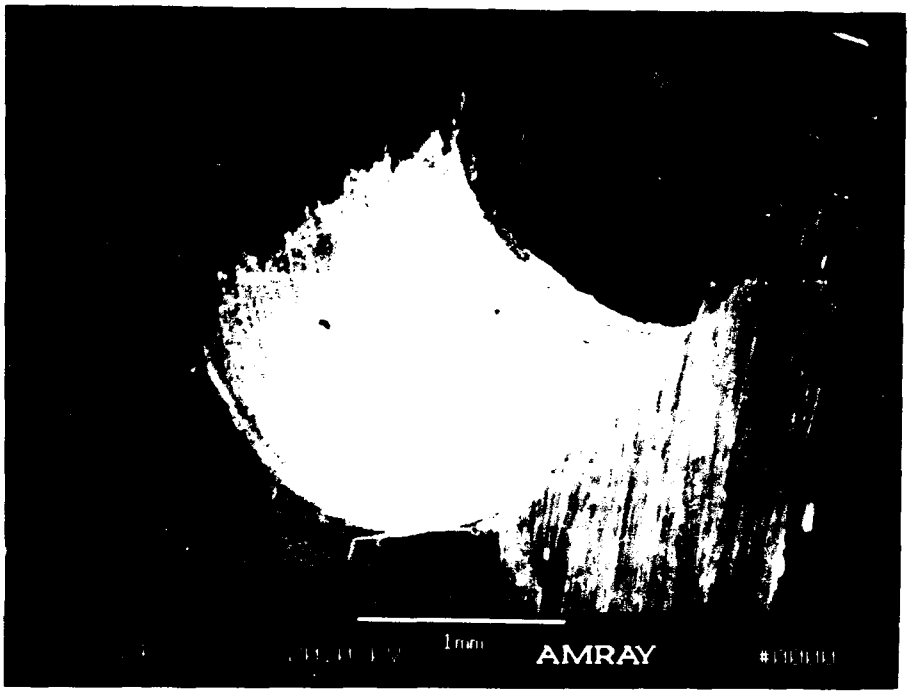

Figure 24 Fracture Surface, $[0]_8$ specimen (90G0509)

brittle surface coating of matrix material on the specimens formed very thin transverse cracks as strain increased. An extreme case of this is shown in Figure 25, where the longitudinal crack has already progressed some distance from the hole and divided the specimen into two portions. The portion of the specimen containing the hole can no longer bear load, and shows little damage. Transverse surface cracks can be seen clearly on the other, load-bearing portion of the specimen, however, showing that it has continued to strain.

The acoustic data for the $[0]_8$ specimens followed a pattern of low activity (mostly test machine noise) until a point where the count rate increased suddenly. This was compared to the results from C-scans of the $[0]_8$ specimens used for incremental tests, which showed that the point of increased acoustic activity corresponded to the point of visible surface damage and initial longitudinal splitting of the specimen around the hole (Figures 26, 27). The C-scan images indicate damage in all plies, suggesting through-cracking; this was confirmed by sectioning the tested specimen. The cut surface of the specimen was polished and cracking through the thickness was observed (Figure 28). The loads corresponding to each point of indicated initial damage are plotted, along with the corresponding ultimate load, in Figure 29. Some of the scatter in replica data is the result of the intervals between

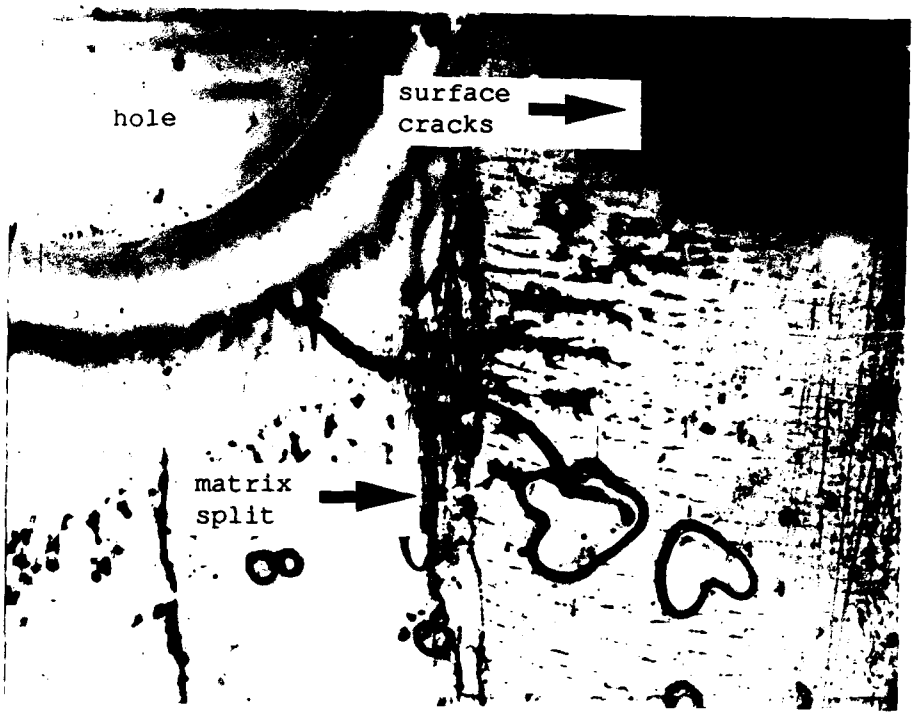

Figure 25 Transverse Surface Cracking in $[0]_8$ Specimen

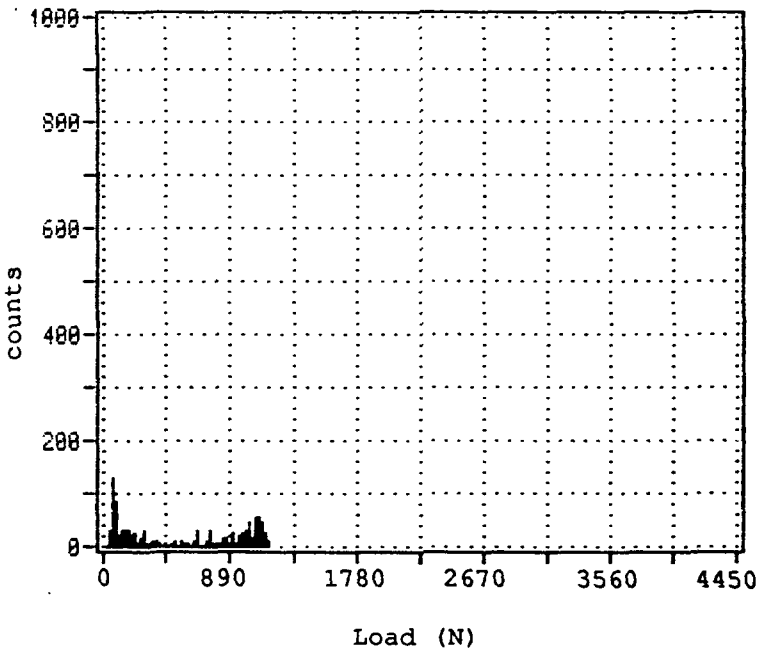

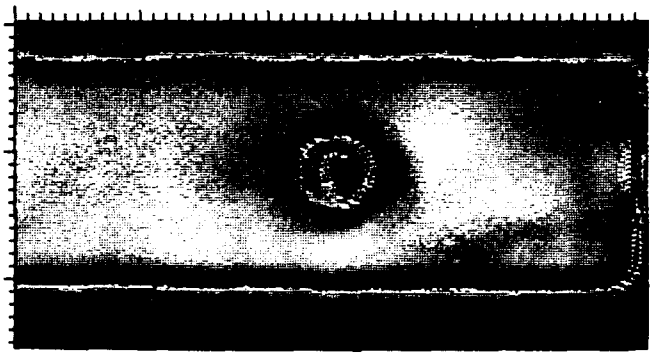

Figure 26 Acoustic Emission and C-Scan Before Damage in Incrementally Tested $[0]_8$ Specimen (90G0502)

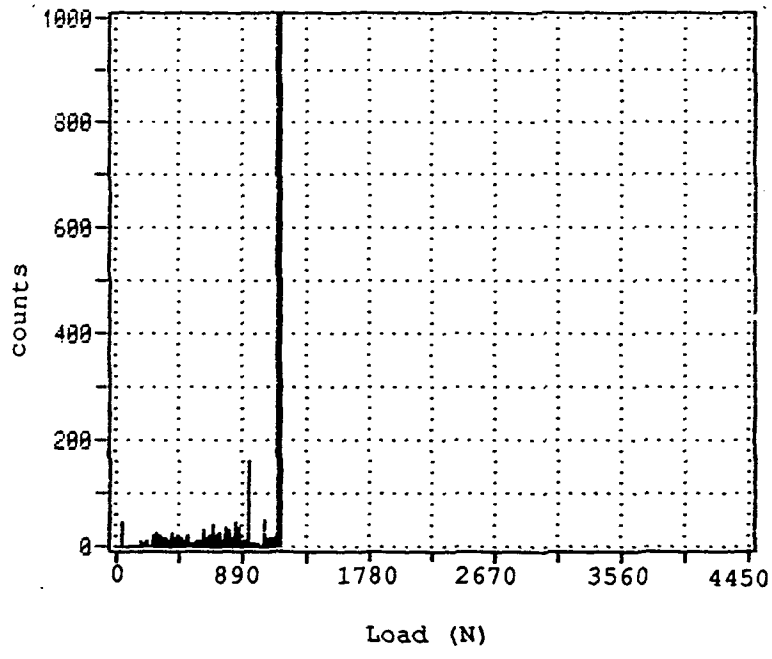

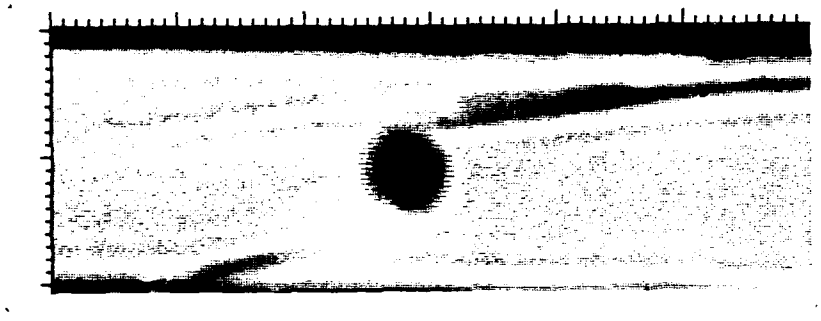

Figure 27 Acoustic Emission and C-Scan After Damage in Incrementally Tested $[0]_8$ Specimen (90G0502)

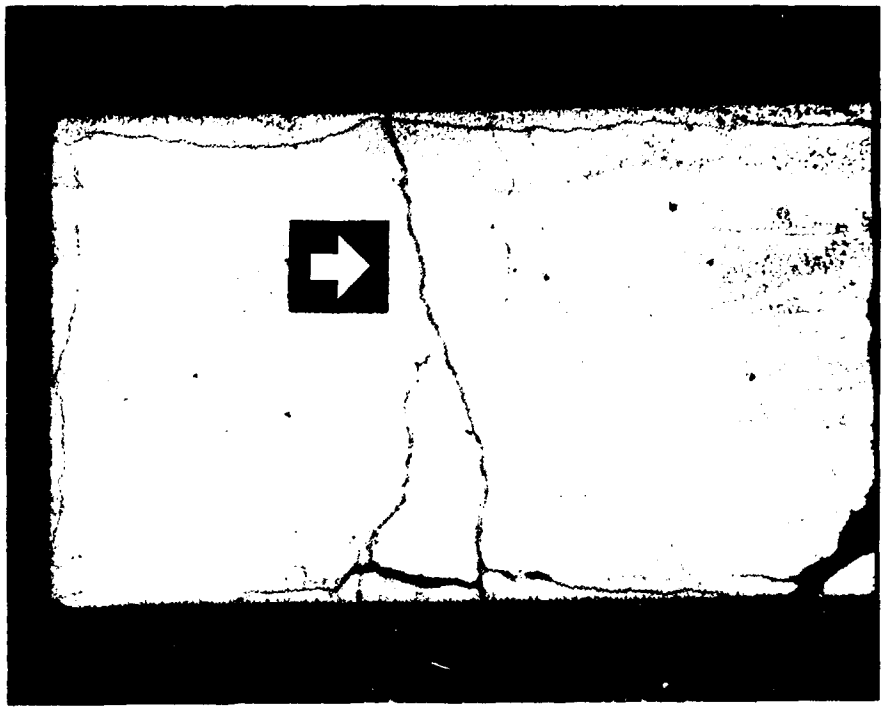

Figure 28 Sectioned Specimen Showing Through Crack (90G0504)

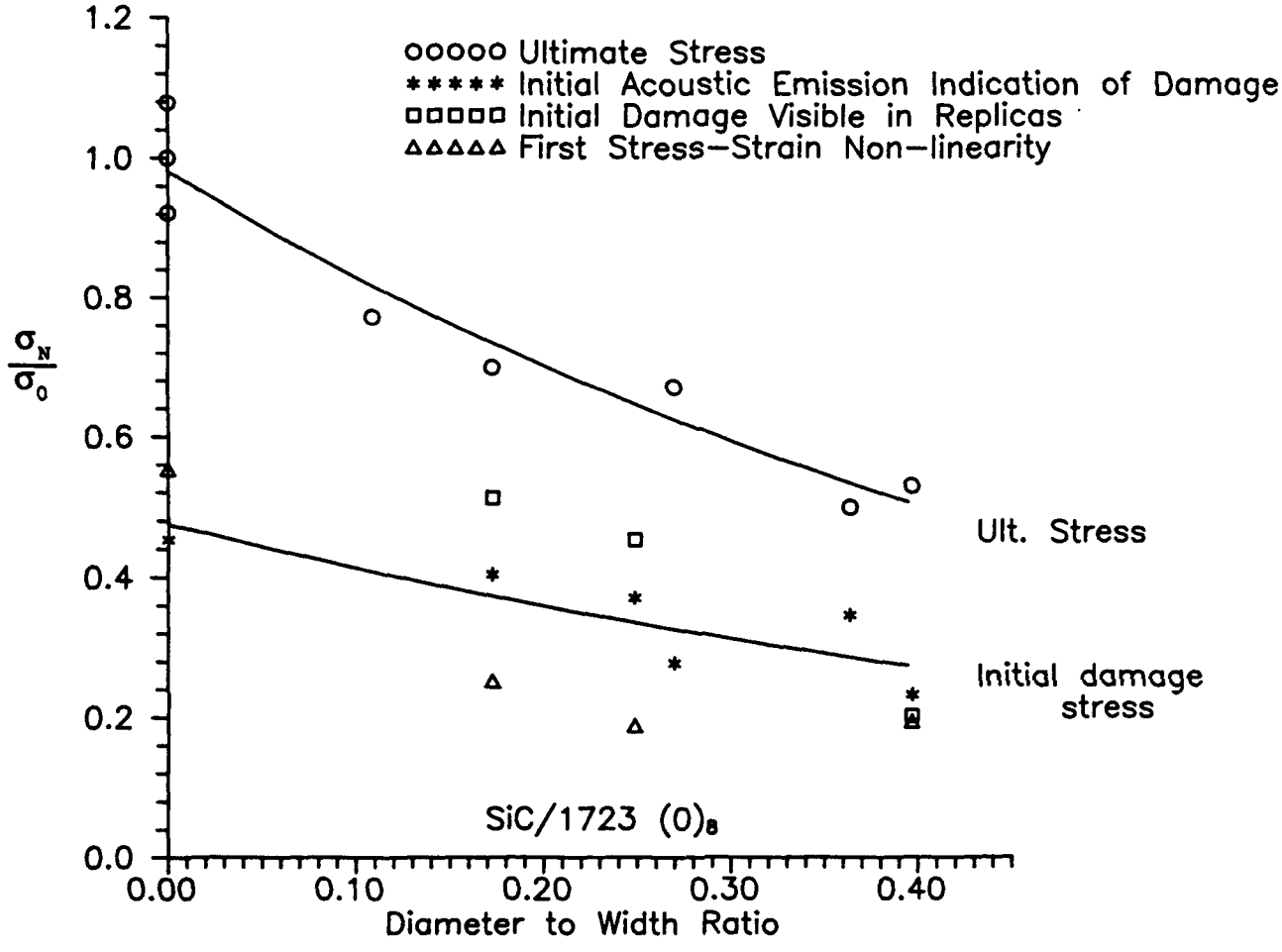

Figure 29 Initial Damage Indication for $[0]_8$ Specimens

taking replicas, which were 220 to 450 N.

Figure 29 indicates that the onset of matrix cracking visible at the surface is in good agreement with the onset of increased acoustic activity, confirming the incremental test findings. The point at which this occurs is roughly one-half the ultimate stress for each D/W ratio, which agrees with the findings of Prewo and Brennan (17) in notched-beam flexural tests on SiC/LAS ceramic matrix composite. Stress-strain curves from gauges near the holes became non-linear somewhat sooner, less than one-half the ultimate stress for both the unnotched (Figure 30) and notched specimens (Figure 31); this suggests that stress-strain nonlinearity near the hole may be the most effective means of determining the point of initial damage in the $[0]_8$ layup. Stress-strain curves from remote gauges usually did not show non-linearity until significantly higher stress levels. This corresponds with the results of Mall & Kim (13), who reported that damage in unnotched ceramic matrix composites (as indicated by AE) occurred well before non-linearities in stress-strain curves were evident. The relative notch-insensitivity and pattern of matrix splitting corresponds to Tan's (18) findings in $[0]_8$ graphite-epoxy specimens. The separation of the specimens into two separate load bearing portions, each without a hole, accounts for the low degree of notch sensitivity. The large degree of

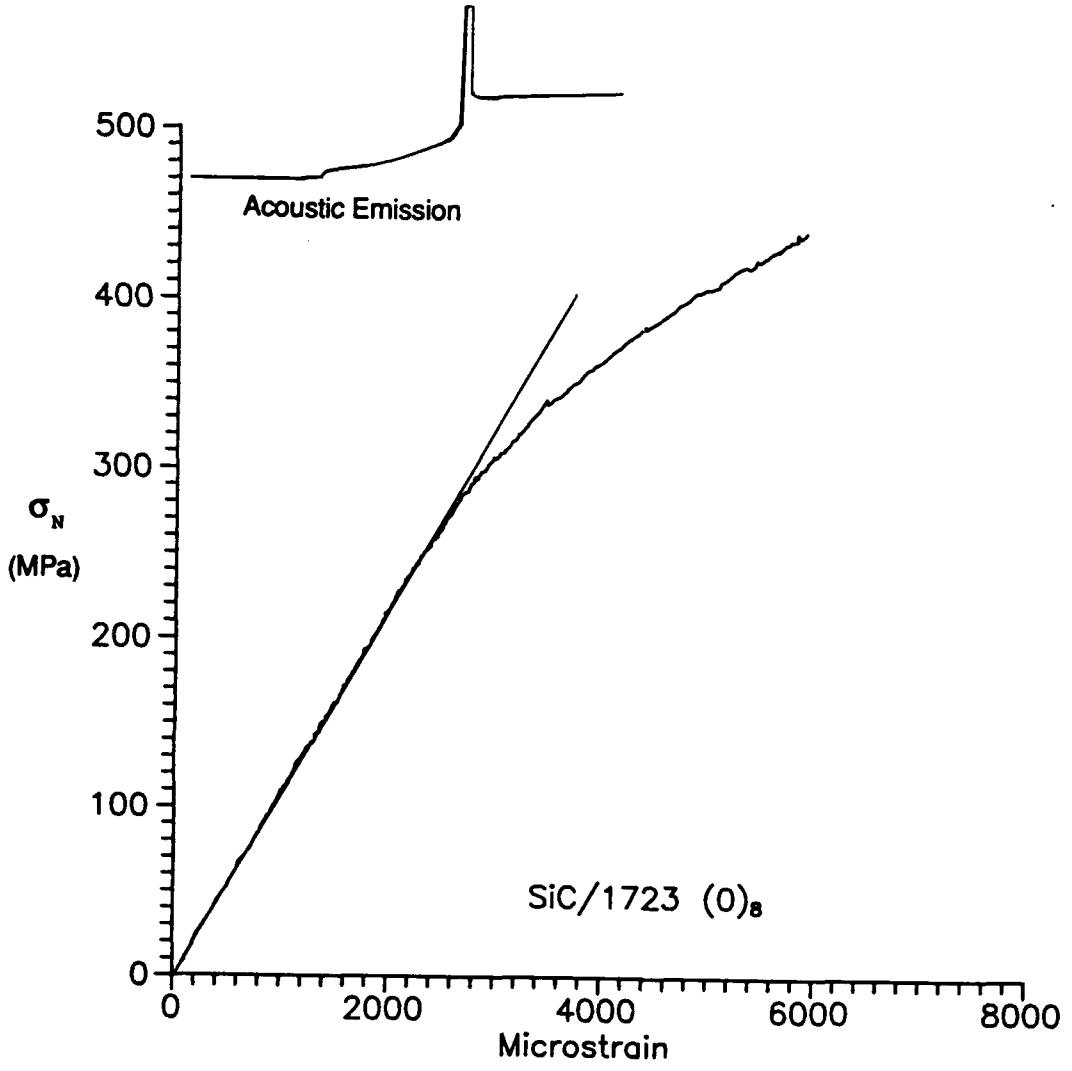

Figure 30 Stress-Strain Curve, Unnotched $[0]_8$ Specimen

(90G0505)

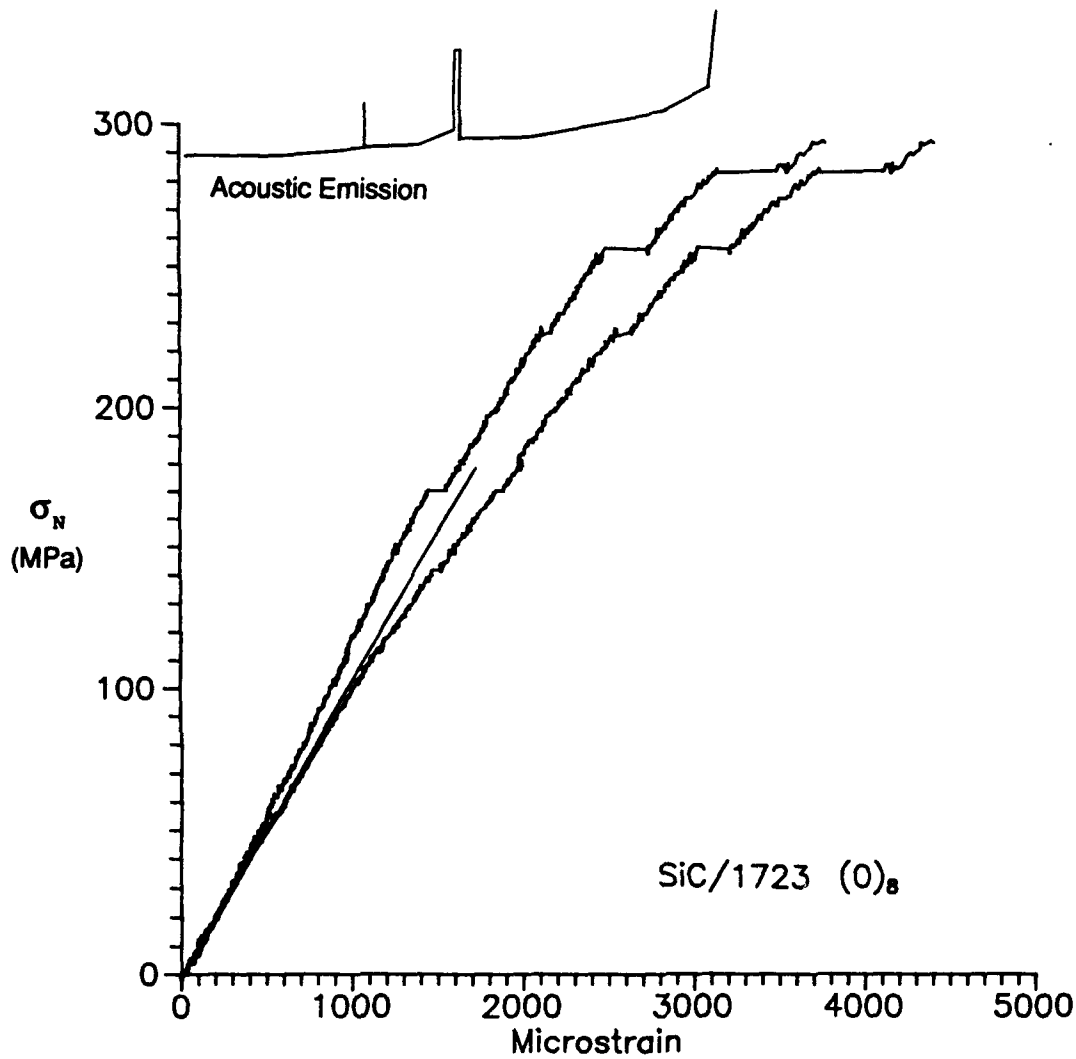

Figure 31 Stress-Strain Curve, Notched $[0]_8$ Specimen (90G0503)

fiber pullout is consistent with the results of Marshall and Evans with SiC/LAS ceramic matrix composite specimens (14).

The axial modulus of elasticity was measured on the specimens without holes, and averaged 105 GPa, very close to the calculated modulus of 107.1 GPa for the unidirectional composite. The transverse modulus and Poisson's ratio were not measured.

These results are compared to the Whitney-Nuismer failure theory discussed in Chapter 2. Whitney and Nuismer (22) used specimens of equal width for their tests, and expressed their results in terms of the radius of the hole (Equations 17 and 19). These equations were modified to permit application to the results of this study, where specimens were of different widths. Equations (17) and (19) were replaced with:

$$\xi_1 = \frac{(D/W)}{\left[\quad) + (D/W)_{d_o} \right]} \tag{29}$$

and

$$\xi_2 = \frac{(D/W)}{\left[(D/W) + (D/W)_{a_o}\right]} \tag{30}$$

where

(D/W) = Hole diameter to width ratio (replacing radius R)

$(D/W)_{do}$ = Characteristic D/W for point stress criterion (replacing Whitney-Nuismer characteristic distance d_o)

$(D/W)_{ao}$ = Characteristic D/W for average stress criterion (replacing Whitney-Nuismer characteristic distance a_o)

This served to normalize the results for different specimen widths. Using this variation on Whitney and Nuismer's procedure, it was found that good agreement with experimental results was achieved with $(D/W)_{do} = 0.084$ for the point stress criterion and $(D/W)_{ao} = 0.232$ for the average stress criterion (Figure 32, 33). These values were determined through a least-squares best fit of the Whitney and Nuismer curve to the experimental data. Since the Whitney-Nuismer theory is based on stresses in infinite plates, the experimental values have been adjusted from finite plate to infinite plate values using Tan's finite width correction factor (Equation (13)).

The results were then compared to the Pipes *et al.* modification to the Whitney-Nuismer theory. This theory is also based on specimens of constant width, so it was also modified to allow application to specimens of varying width. The radius R was replaced with the diameter-to-width ratio (D/W). Also, in Pipes' theory, the reference radius R_o is introduced merely to non-dimensionalize the radius R, and is typically set equal to one unit (one inch, one cm, etc.) for

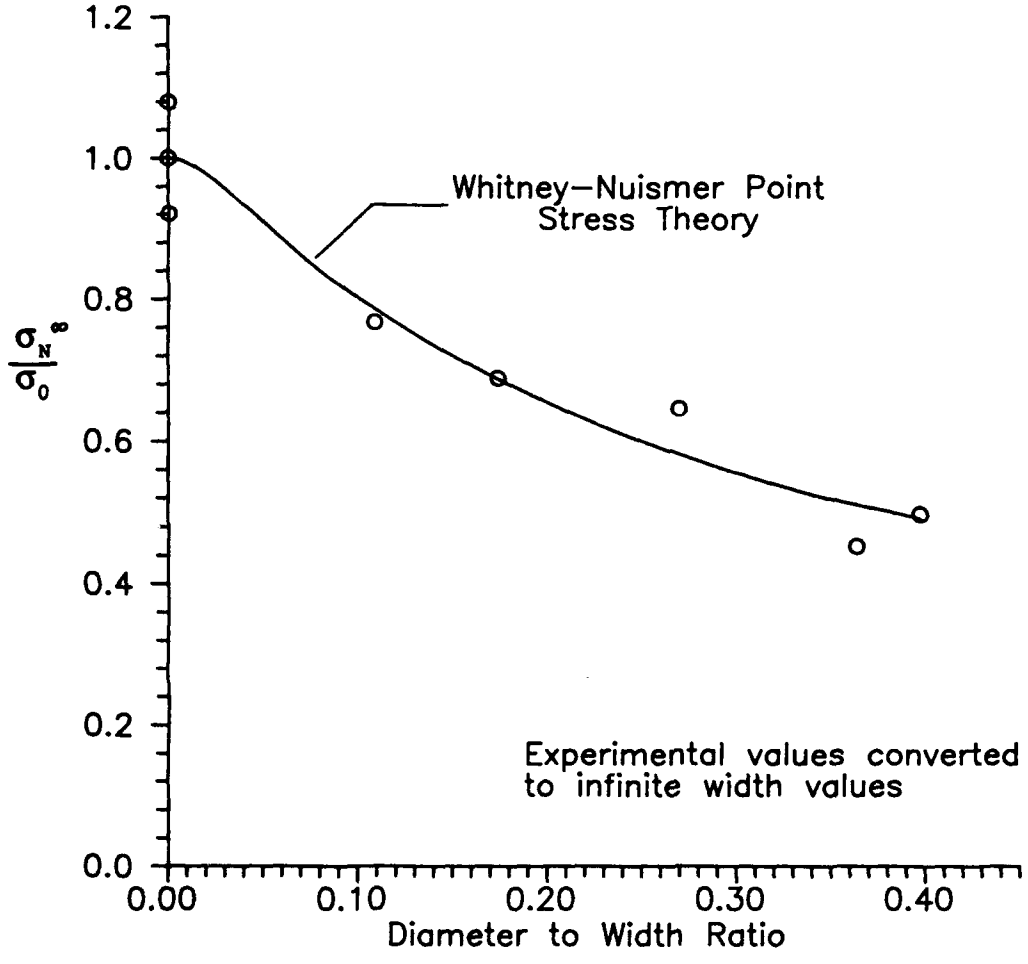

Figure 32 Comparison of Whitney-Nuismer Point Stress Criterion to Experimental Results ($[0]_8$)

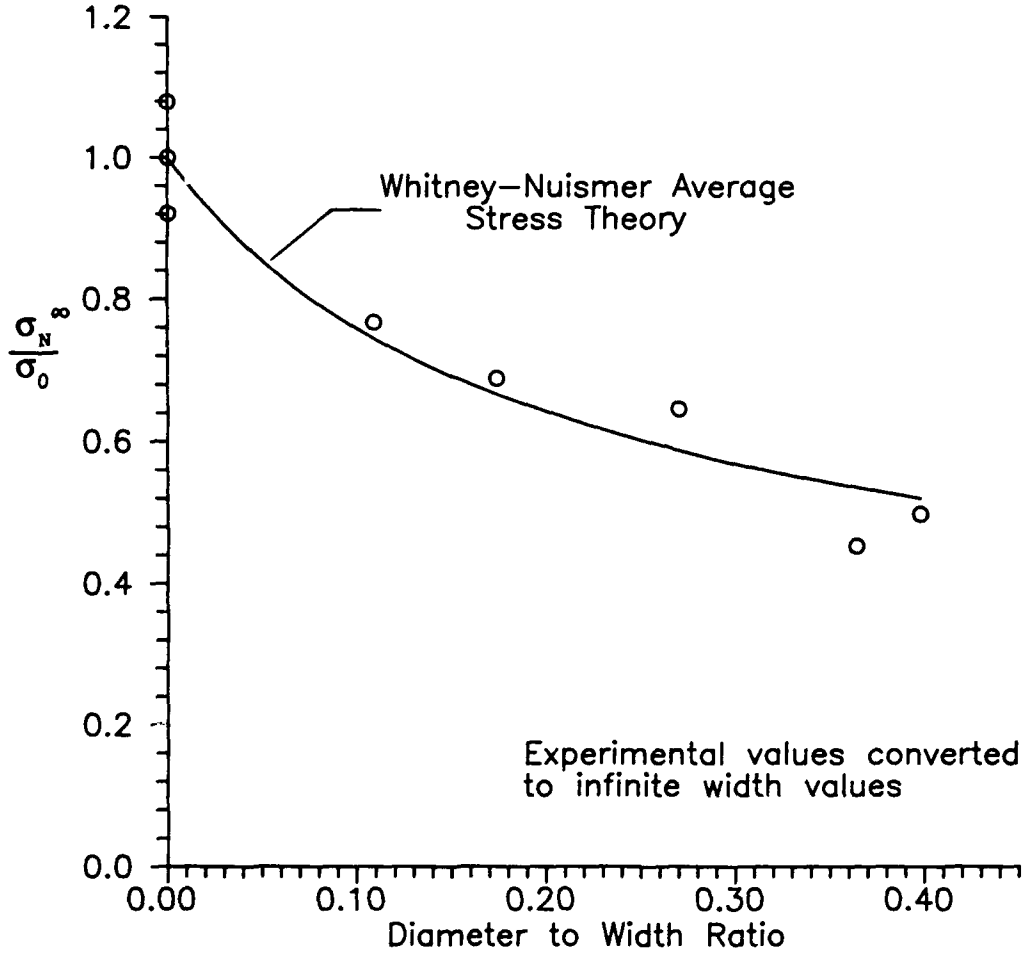

Figure 33 Comparison of Whitney-Nuismer Average Stress Criterion to Experimental Results ($[0]_8$)

algebraic convenience. Since D/W is already dimensionless, R_o is eliminated here. Thus, Equations (21) and (23) were changed to:

$$d_o = \frac{(D/W)^m}{C} \tag{31}$$

and

$$\lambda = [1 + (D/W)^{m-1} C^{-1}]^{-1} \tag{32}$$

respectively. These were then used to solve Equation (22). It was found that the best fit to the experimental data (determined by least-squares error minimization) was with an exponential parameter m of zero and a notch sensitivity parameter C of 11.9 cm^{-1}. Since m = 0, the Whitney-Nuismer curve is recovered, so the Pipes *et al.* theory does not improve the prediction of ultimate stress for this layup. By comparison, Pipes *et al.* found the notch sensitivity parameter C to range from 19 cm^{-1} for [+45/-45/0/90]S graphite-epoxy to 75 cm^{-1} for unidirectional boron-aluminum. The relatively low value of C for this layup is consistent with its low degree of notch sensitivity.

One specimen, 90G0509, failed at a much higher stress than anticipated. The specimen was prepared with longer tabs than the other unidirectional specimens (1.9 cm vs. 1.3 cm) with a smaller tab angle (15° vs. 45°) (Figure 34). Cunningham *et al.* (6) studied the effect of

tab design, and found in experiments on cross-plied graphite-epoxy that varying the length of a tab had little effect on failure stress, but a change in angle from 45 ° to 10° increased the failure stress 25%. It is believed that the large discrepancy in failure stress for this one specimen may be due to the difference in tab geometry. Only data from specimens with 1.3 cm tabs were used for ultimate stress analysis.

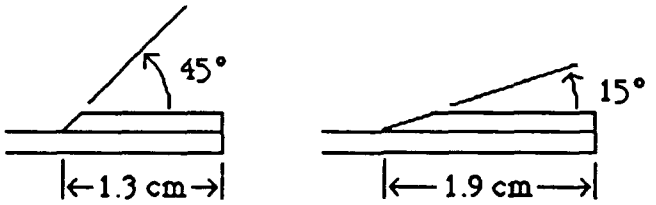

Figure 34 Variation in Specimen Tab Configuration

b. $[0/90]_{2S}$ (Cross-Ply) Laminate

Seven specimens of the $[0/90]_{2S}$ layup were successfully tested to failure (some specimens broke prematurely at the grips instead of at the hole, but were not used for this analysis). In addition, four $[0/90]_{2S}$ specimens were tested to failure by Moschelle (15). These additional specimens were of the same material and layup, but from a different plate, numbered 91G01. This plate, like the others, was manufactured in the Air Force Materials Laboratory. All eleven test specimens were

prepared in the same manner, with the same length and end tab geometry. The ultimate unnotched and notched area stresses for all eleven specimens are shown in Table 3. The failed specimens are illustrated in Figure 35. The ultimate unnotched area stresses σ_N are plotted as a function of D/W ratio in Figure 36, and the ultimate notched area stresses σ_N^N as a function of D/W ratio in Figure 37. As is the case for the $[0]_8$ layup, the straight line in Figure 36 is the line of net strength, along which stress on the notched cross-sectional area is constant. The ultimate stress for each specimen is normalized by dividing it by the average value of all unnotched specimens from the

Table 3 Ultimate Stresses ($[0/90]_{2S}$ Layup)

Specimen Number	Diameter-to-Width Ratio	Ultimate Unnotched Area Stress σ_N (MPa)	Ultimate Notched Area Stress σ_N^N (MPa)
91G0205	0	264.2	264.2
91G0206	0	268.7	268.7
91G0102	0	254.0	254.0
91G0112	0	226.0	226.0
91G0210	0.143	214.8	250.6
91G0106	0.260	165.0	223.0
91G0111	0.260	160.6	217.0
91G0203	0.264	211.8	287.8
91G0211	0.364	161.6	254.0
91G0209	0.377	169.9	272.7
91G0202	0.387	175.2	285.9

Figure 35 Failed $[0/90]_{2S}$ Specimens

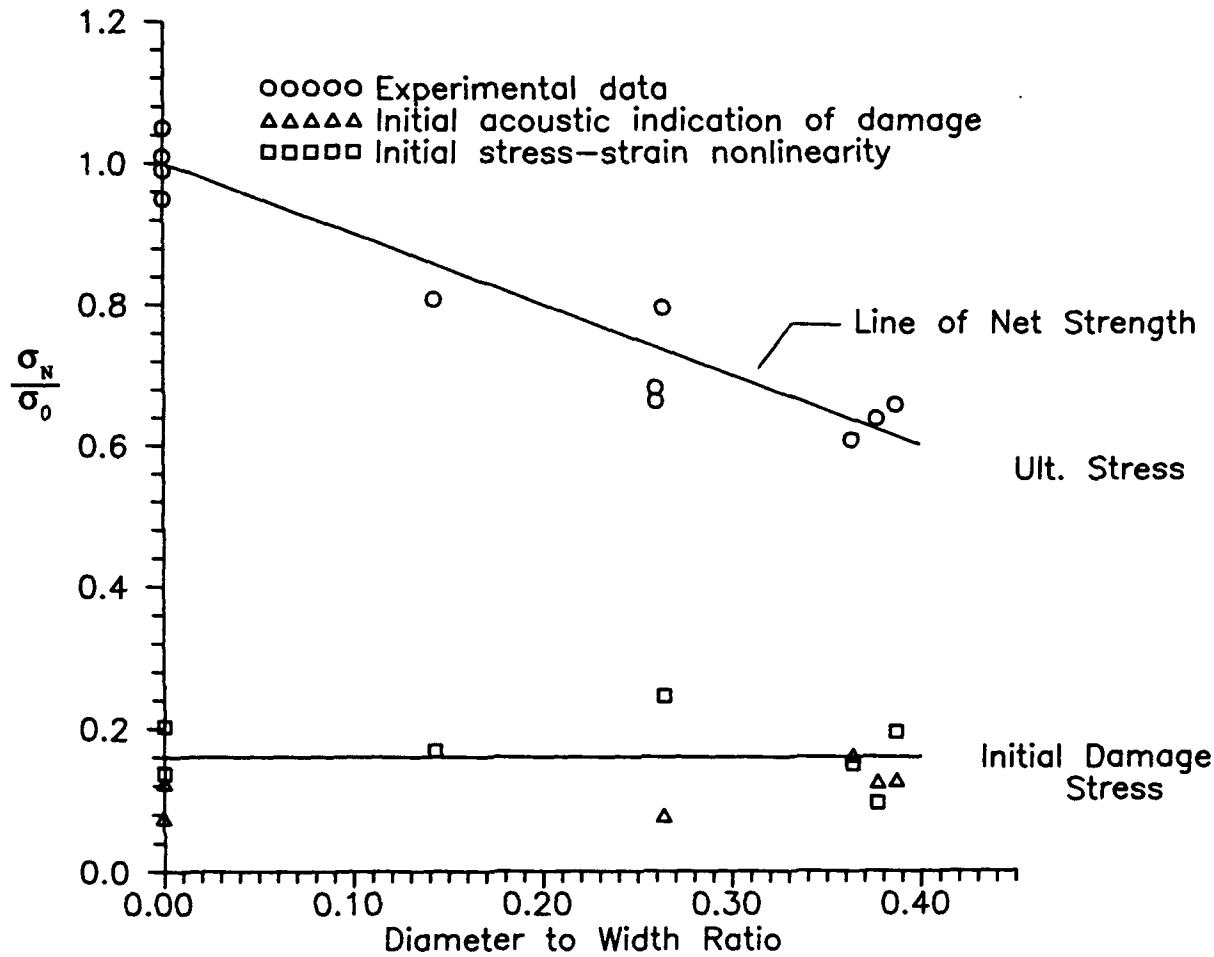

Figure 36 Ultimate Unnotched Area Stress as a Function of D/W Ratio, $[0/90]_{2S}$

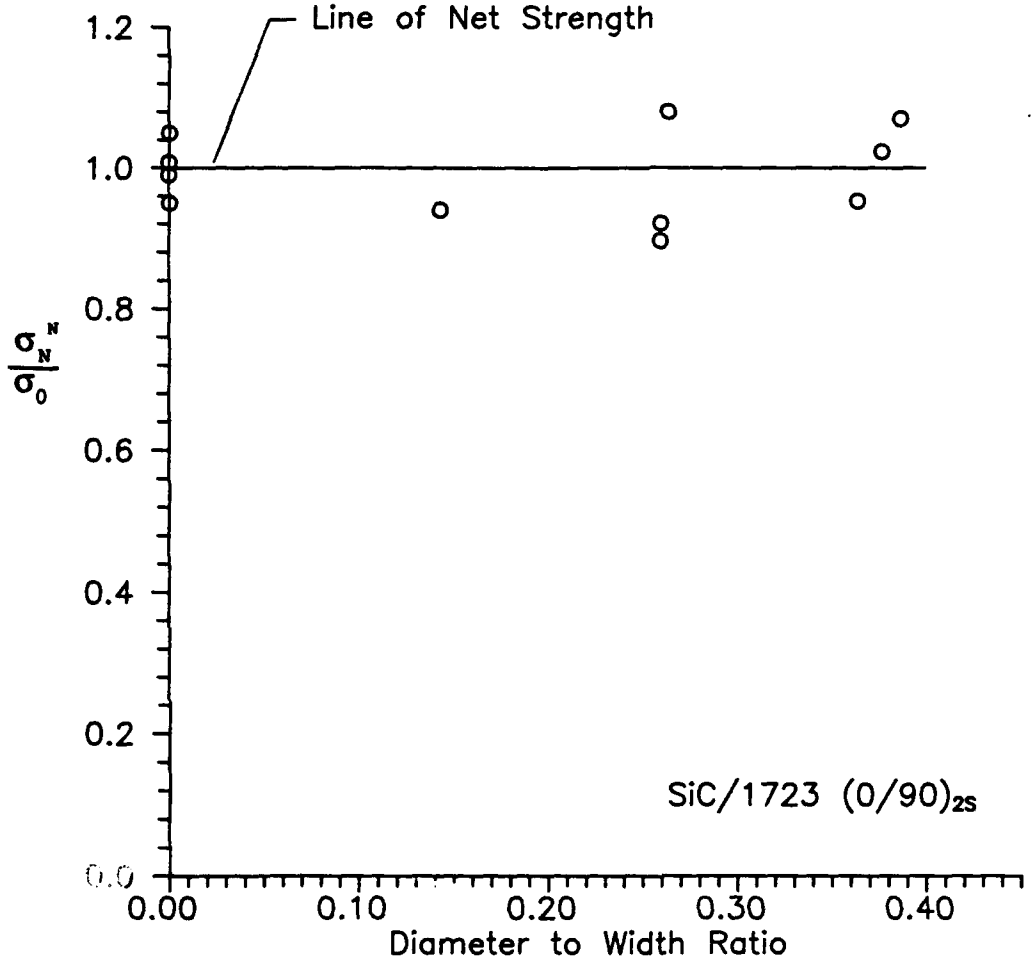

Figure 37 Ultimate Notched Area Stress as a Function of D/W Ratio, $[0/90]_{2S}$

same plate. Unnotched specimens from plate 91G02 averaged an ultimate stress of 266.5 MPa, while those from plate 91G01 averaged 240 MPa.

These plots show that the $[0/90]_{2S}$ layup is notch-insensitive to an even greater degree than the $[0]_8$. The best fit curve coincides with the line of net strength, indicating no effect of any stress concentration at the hole on the ultimate stress. This can be interpreted as a 0% notch sensitivity for this layup. This is consistent with the results of Chang *et al.* (5) with a $[(0/90)_4]_S$ layup of graphite-epoxy; they found the ultimate notched area stress for a specimen with D/W = 0.33 nearly the same as (actually slightly higher than) that for a specimen with D/W = 0.25.

The specimens broke transversely in the region of the hole; the 90° plies showed brittle fracture of the matrix between fibers, and the 0° plies showed significant fiber pullout (Figures 38, 39).

In the $[0/90]_{2S}$ layup, the acoustic activity was characterized by a period of very low activity, followed by a sudden rise in count rate at a low stress level (typically 20-50 MPa) and an increase in amplitude to the limit of the instrumentation (100 dB). At a higher load, the count rate decreased slightly, then increased again near failure. This appears to indicate onset of transverse matrix cracking activity near the hole, where the stress is greatest, followed by a lower level of

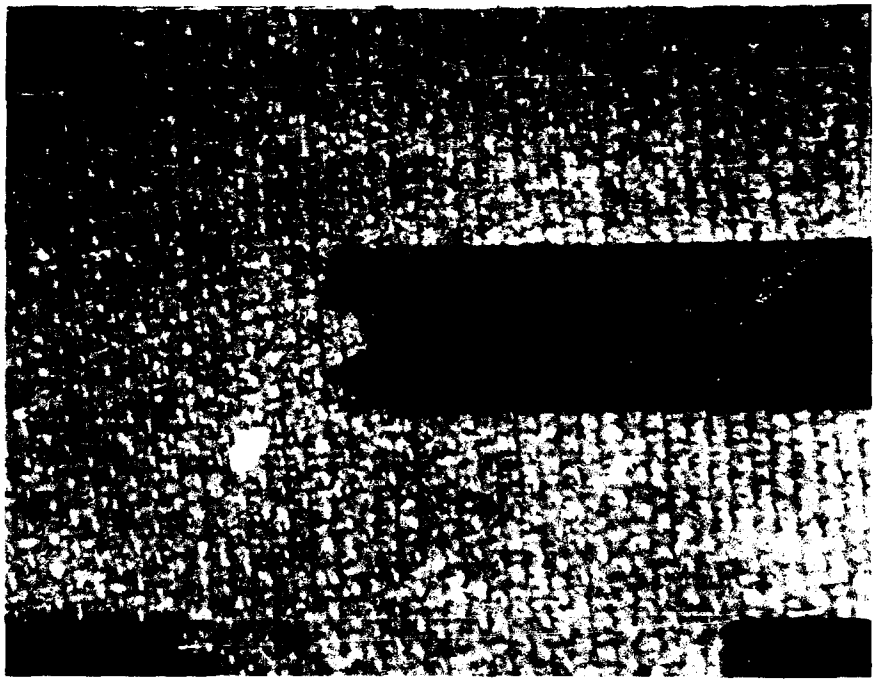

Figure 38 Typical Failed $[0/90]_{2S}$ Specimen (91G0203)

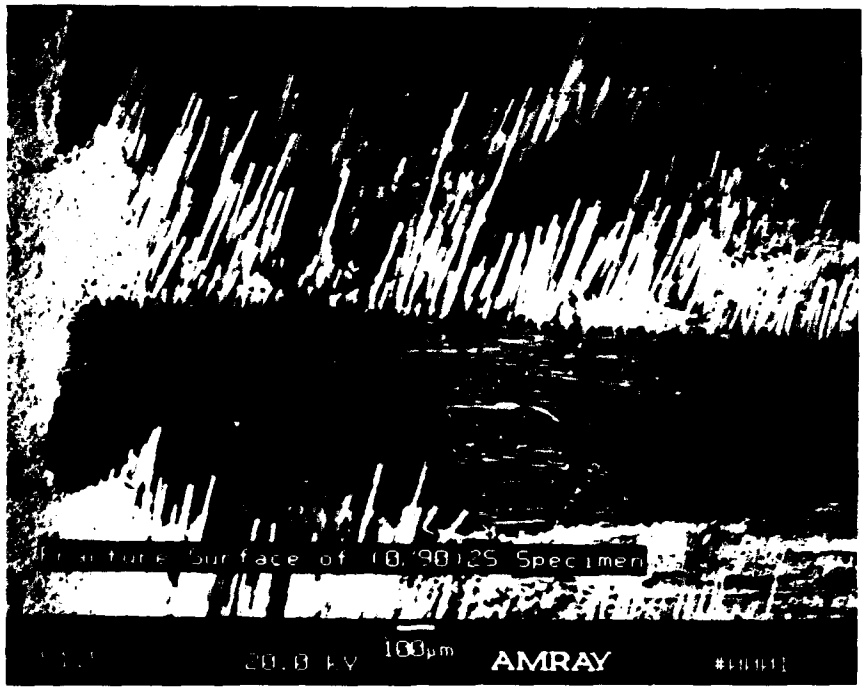

Figure 39 Fracture Surface, $[0/90]_{2S}$ Specimen (91G0210)

activity as the load increases toward ultimate, ending with renewed acoustic activity as the 0° fibers begin to fail. The replicas show transverse matrix cracks appearing at the edge of the specimen at nearly the same stress as indicated by acoustic emission, suggesting the cracks, once started, propagate immediately through the 90° plies (Figures 40, 41). C-scans also confirm that the initial acoustic activity corresponds to the initiation of these transverse cracks.

Non-linearity of stress-strain curves from the gauges adjacent to the holes is evident at approximately the same stress level as indicated by the other methods for initial transverse cracking. Both unnotched and notched specimens show initial nonlinearity in the stress-strain curve at approximately 15 to 20 percent of ultimate stress (Figure 42, Figure 43, Fig. 44). By comparison, Mall and Kim (13) reported that AE activity significantly preceded changes in the slope of the stress-strain curves in [0/±45/90]S ceramic matrix composites. That study was conducted with unnotched specimens where damage would be expected to be evenly distributed throughout each specimen. In this study, the strain gauge was placed adjacent to the hole at the point of greatest stress concentration, and could therefore reflect initial damage occurring at that location. This placement accounts for the effectiveness of strain gauges by the hole. In contrast, the gauges placed remote from the hole

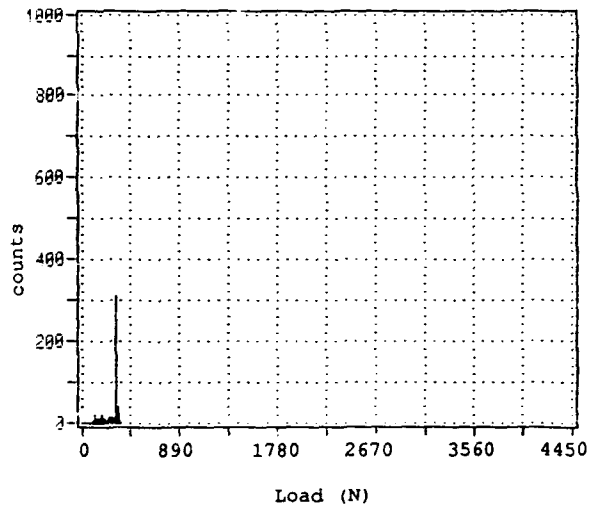

Figure 40 Acoustic Emission and Edge Replica Before Damage

(91G0207)

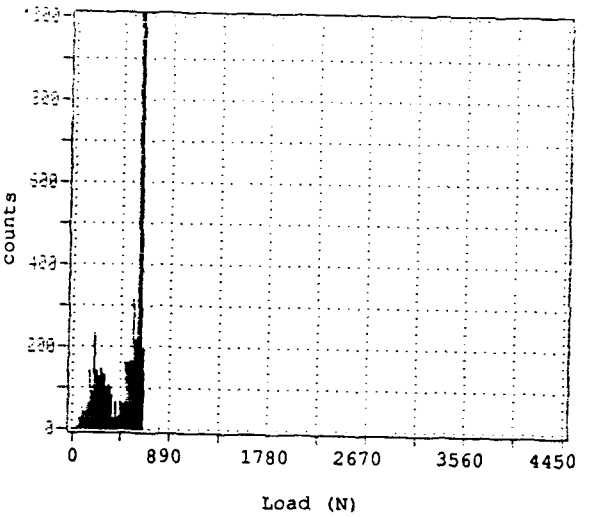

Figure 41 Acoustic Emission and Edge Replica After Damage

(91G0207)

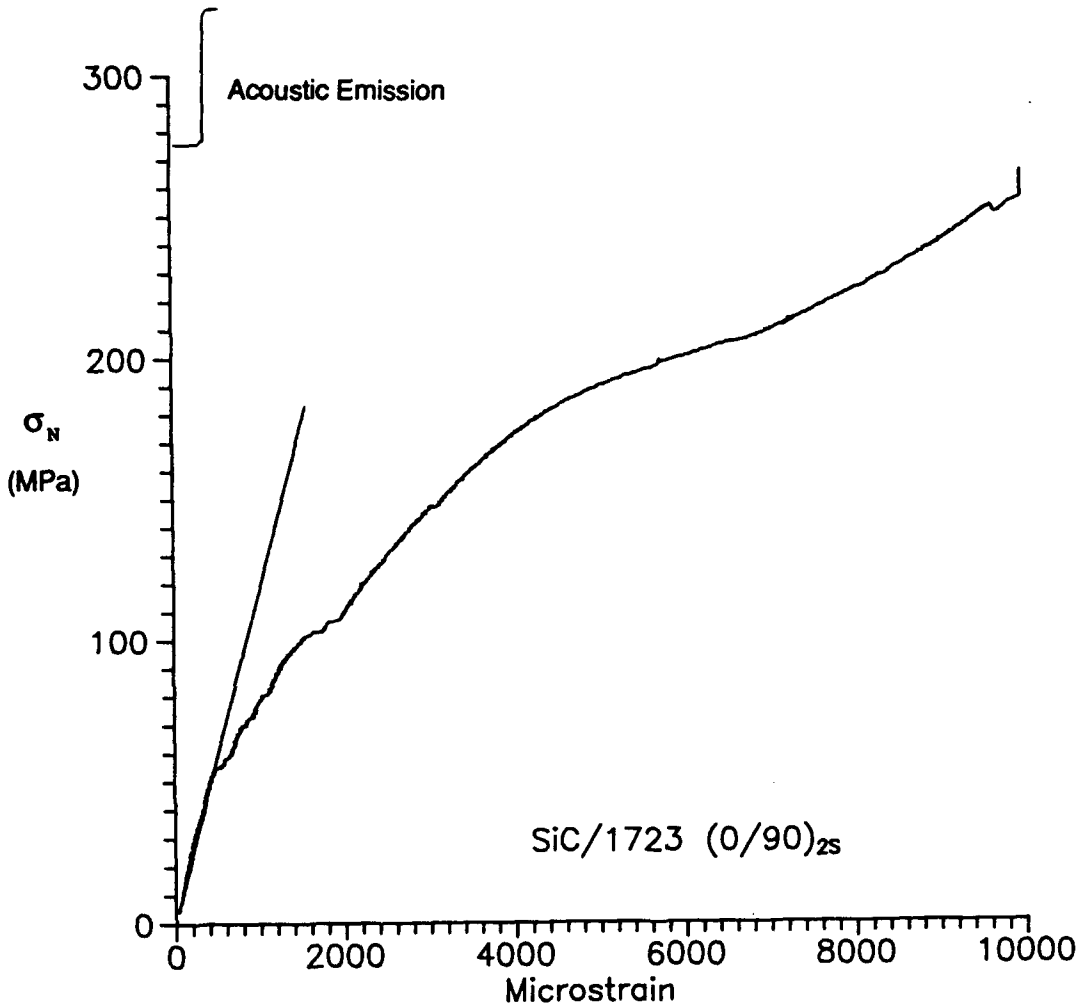

Figure 42 Stress-Strain Curve for Unnotched $[0/90]_{2S}$ Specimen

(91G0205)

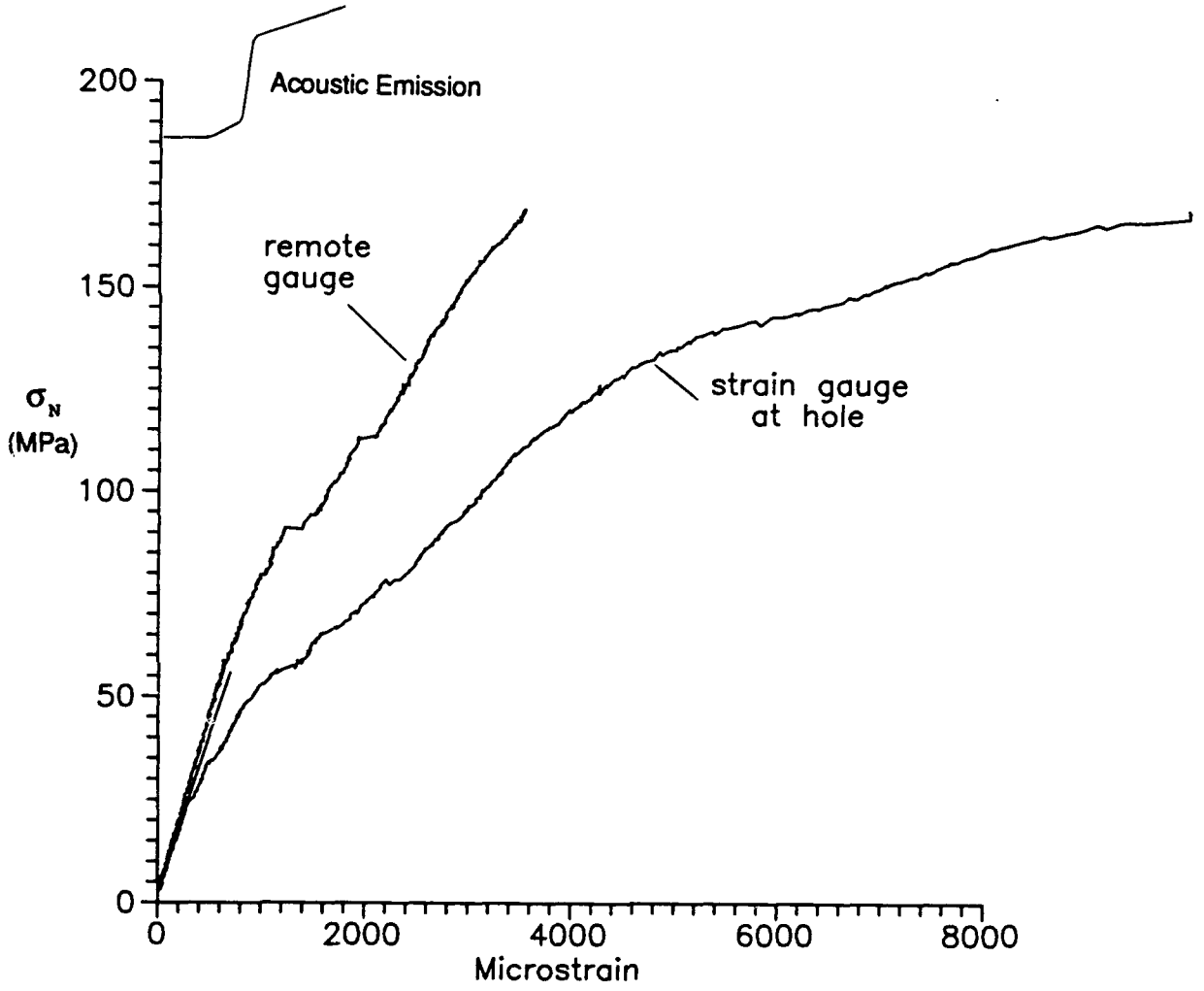

Figure 43 Stress-Strain Curve for Notched $[0/90]_{2S}$ Specimen

(91G0209)

did not accurately reflect initiation of damage. Also, for most of the specimens, there appears to be a second linear region of stress vs. strain between the first non-linearity and a second near failure. This is also measured from the strain gauge adjacent to the hole (Figure 44). If the 90° plies are no longer contributing toward stiffness near the hole, it is reasonable to expect the 0° plies to act linearly throughout their elastic range.

These results make it possible to describe the sequence of damage progression. The failure of the $[0/90]_{2S}$ specimens began with transverse matrix cracking in the 90° plies in the region of the hole at very low stress levels, when the transverse layer experienced the matrix's ultimate strain. These cracks propagated quickly, due to the brittleness of the material, to the outer edge of the specimen. As load increased, additional transverse matrix cracks formed, and the 90° plies could be discounted in the region of the hole. The entire load was transferred to the 0° plies, which cracked longitudinally in the region of the hole (as described above for the $[0]_8$ specimens). This resulted in separation of the specimen into load carrying portions on either side of the hole. The ultimate stress was entirely notch-insensitive since the load carrying portions no longer included a stress concentration. Final failure occurred due to breakage in tension of the 0° fibers.

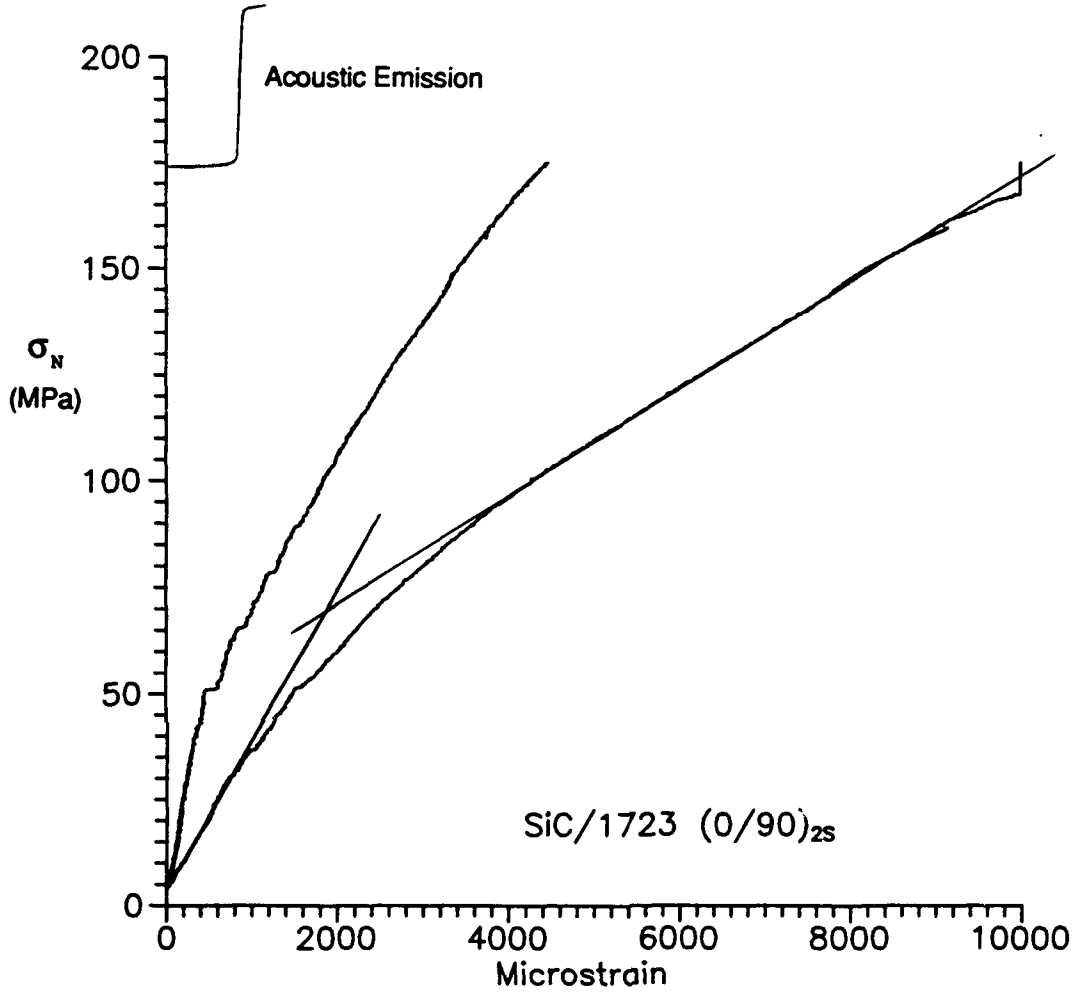

Figure 44 Stress-Strain Curve Showing Second Linear Portion

(91G0202)

This is consistent with the findings of Chang *et al* in $[0/90]_{6S}$ graphite-epoxy specimens (5).

The modulus of the $[0/90]_{2S}$ specimens without holes averaged 76 GPa. Since the actual transverse modulus (E_2) of the unidirectional material was not measured, this experimental result could not be confirmed directly; the rule of mixtures approach used in Equation (25) assumes perfect bonding between fibers and matrix, and experimental values are typically lower. Therefore, it is reasonable to expect the experimental value to be slightly lower than the theoretical value of 95.9 GPa.

As was done for the $[0]_8$ specimens, these $[0/90]_{2S}$ results are compared to the Whitney-Nuismer (22) theory, adjusted for varying width specimens as described above (Equations (29) and (30)). Using this variation on Whitney and Nuismer's procedure, it was found that a least-squares best fit to the experimental data gave $(D/W)_{do} = 0.120$ and $(D/W)_{ao} = 0.333$, which resulted in a curve which agreed well with experiment (Figure 45, 46). The experimental values have been adjusted from finite plate to infinite plate values using Tan's finite width correction factor (Equation (13)).

The Pipes *et al.* (16) theory was also applied to the $[0/90]_{2S}$ results. The same modification was used to allow for specimens of

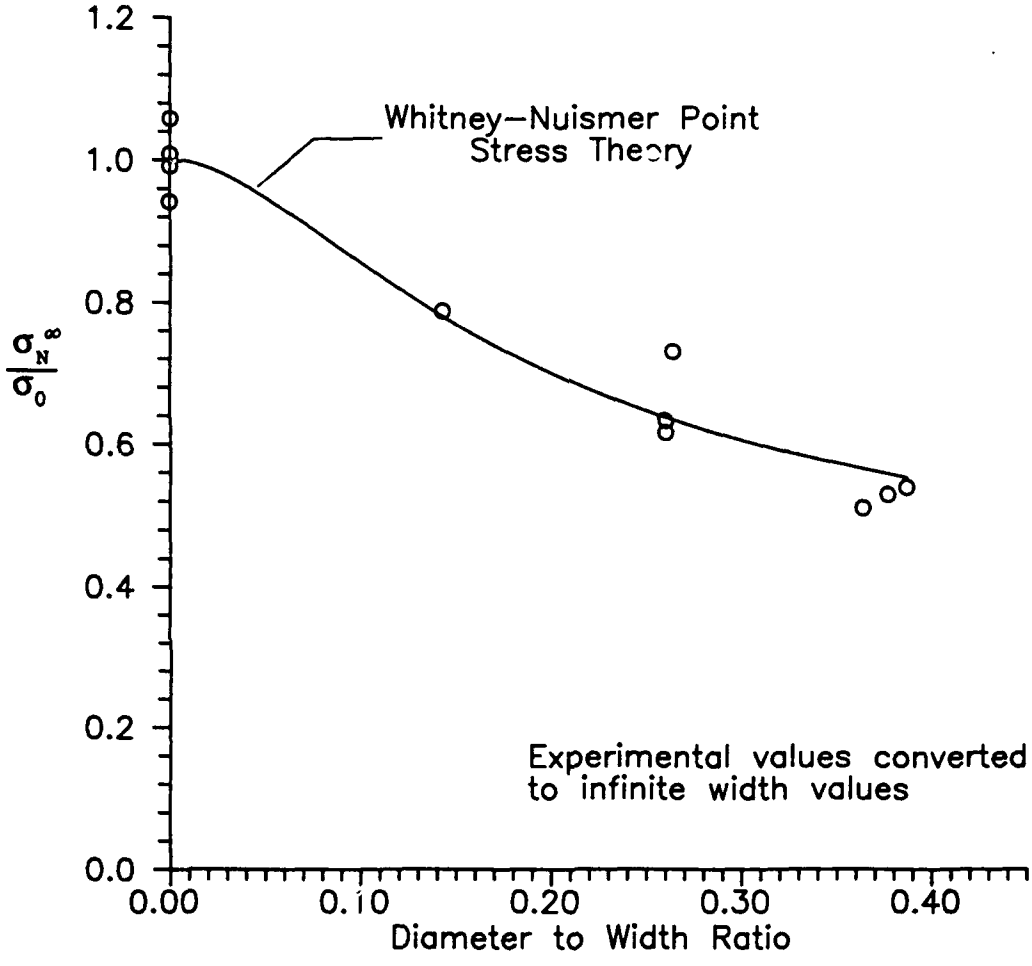

Figure 45 Comparison of Whitney-Nuismer Point Stress Criterion to Experimental Results ($[0/90]_{2S}$)

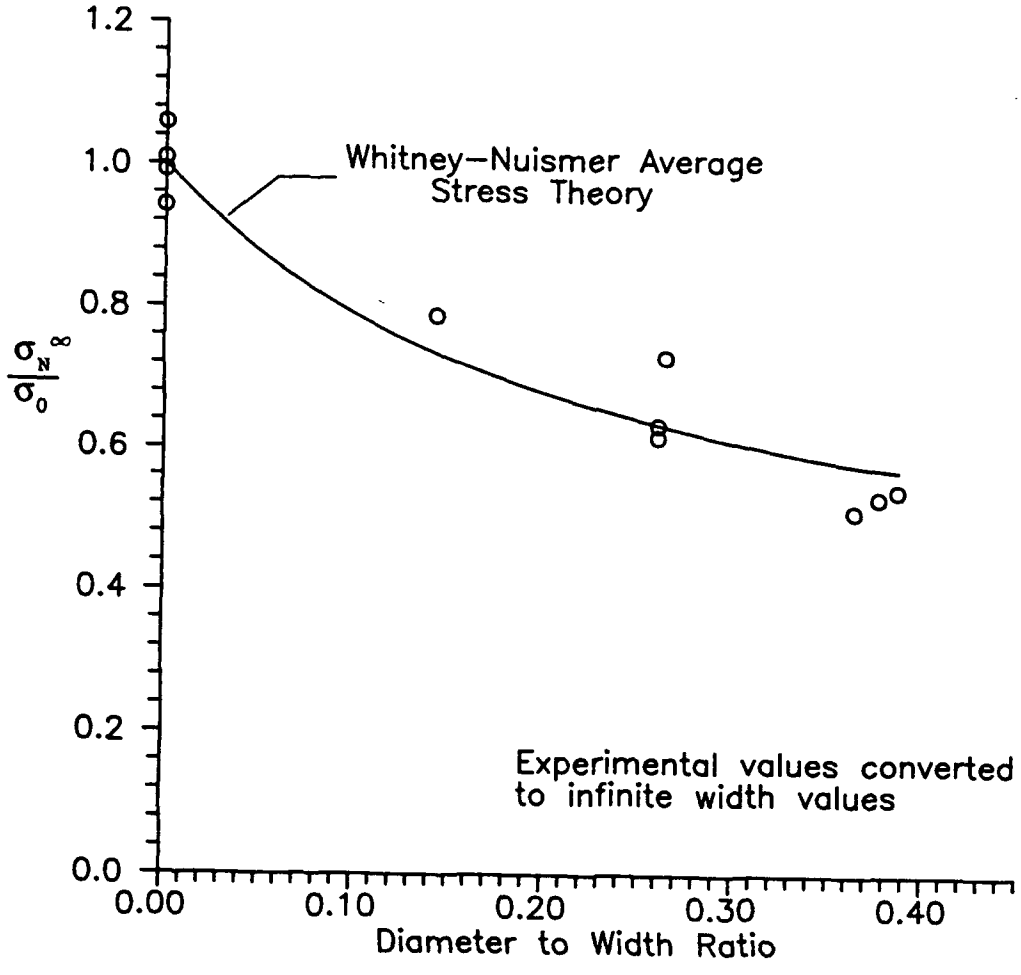

Figure 46 Comparison of Whitney-Nuismer Average Stress Criterion to Experimental Results ($[0/90]_{2S}$)

differing width (Equations (31) and (32)). The best fit to the experimental data (determined by least-squares error minimization) was with an exponential parameter m of zero and a notch sensitivity parameter C of 8.4 cm^{-1}. Since m = 0, the Whitney-Nuismer curve is again recovered, so the Pipes *et al.* theory does not improve the prediction of ultimate stress for either the $[0]_8$ or the $[0/90]_{2S}$ layups. Since a lower value of C indicates less notch sensitivity in the Pipes *et al.* theory, the $[0/90]_{2S}$ layup is less notch sensitive than the $[0]_8$ (C = 8.4 and 11.9, respectively). This is consistent with the difference in notch sensitivity between the two layups observed from Figures 32, 33, 45, and 46.

Comparison of $[0]_8$ and $[0/90]_{2S}$ Results

The unidirectional $[0]_8$ layup was found to be more notch sensitive than the $[0/90]_{2S}$ cross-ply layup. A direct comparison of the best fit curves for ultimate unnotched area stress σ_N is given in Figure 47. The different performance of the two layups was quantified in two ways: by the percentage of notch sensitivity at D/W = 0.4 (16% for $[0]_8$ and 0% for $[0/90]_{2S}$); and by the Pipes *et al.* notch sensitivity factor C (11.9 for $[0]_8$ and 8.4 for $[0/90]_{2S}$). The Whitney-Nuismer point-stress criterion yielded a characteristic ratio $(D/W)_{do}$ equal to 0.084 for $[0]_8$

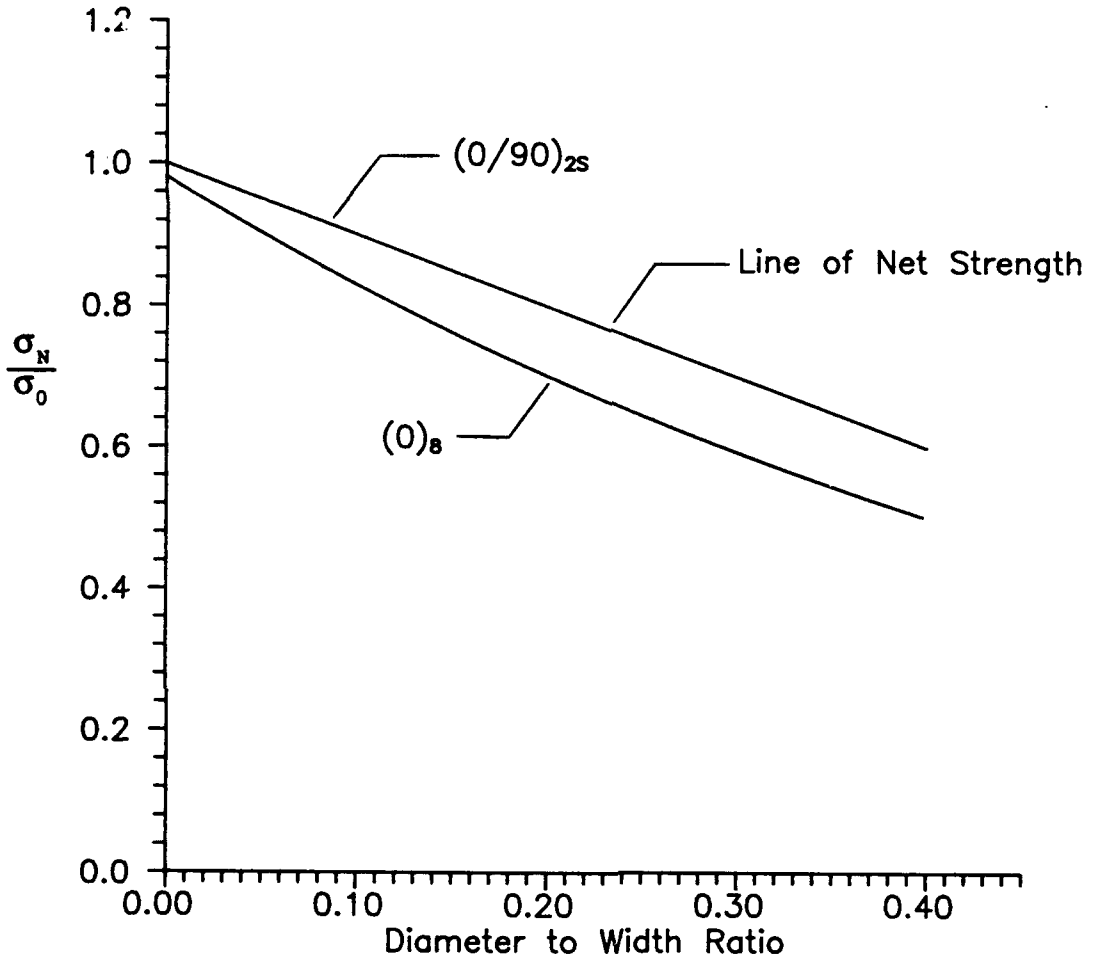

Figure 47 Comparison of Ultimate Unnotched Area Stress for $[0]_8$ and $[0/90]_{2S}$ layups

and 0.120 for $[0/90]_{2S}$. The Whitney-Nuismer average stress criterion gave a ratio $(D/W)_{ao}$ of 0.232 for $[0]_8$ and 0.33 for $[0/90]_{2S}$. This suggests that the $[0/90]_{2S}$ layup experiences a higher percentage of ultimate stress in the region of the hole than the $[0]_8$. before failure, since the characteristic ratios are larger. However, because of the brittle failure patterns of both layups, these ratios may not be indicative of the size of the damage zone. The average ultimate strength of the $[0/90]_{2S}$ unnotched material was approximately 50% of that for the $[0]_8$ layup. This was expected, since after the 90° transverse plies have cracked, the 0° axial plies bear all the load, and the axial plies make up one half the cross-sectional area in the $[0/90]_{2S}$ layup.

Conclusions

This study investigated the performance of a ceramic matrix composite with a circular hole under uniaxial tensile load. The objective was to determine the relationship between failure stress and the ratio of hole diameter to specimen width, the relationship between the stress at which damage initiates and the diameter-to-width ratio, and to examine how damage progresses from initiation toward failure. The ceramic matrix composite used was SiC/1723, composed of silicon titanium carbide fibers in an aluminosilicate glass ceramic matrix. Room temperature tensile tests were performed on two different layups: unidirectional $[0]_8$, and $[0/90]_{2S}$ symmetric. Damage data were gathered using acoustic emission, strain gauges, replication techniques, and ultrasound (C-scan). Two theoretical approaches to predicting failure stress for specimens with circular holes were presented and compared to the experimental data. Several conclusions can be drawn from the results of this study:

1. This material is largely notch insensitive in the $[0]_8$ layup, and entirely notch insensitive in the $[0/90]_{2S}$ layup. This can be seen by the nearly equal notched-area failure stresses for each layup, regardless of the hole diameter-to-width ratio. For the $[0/90]_{2S}$ layup,

failure stress of a specimen with a circular hole can be accurately predicted simply by computing the notched cross-sectional area and applying the failure stress from an unnotched specimen.

2. The failure mode for the $[0]_8$ layup is longitudinal matrix splitting, initiating at a small angle from the opening edge of the hole on the axis normal to the load. Once these cracks start, the specimen is divided into two unnotched load-bearing portions. This elimination of the hole as a source of stress concentration is the reason for this layup's low notch sensitivity. Failure then usually occurs at the grips, which is the area of highest stress concentration. It is believed the effects of grip pressure and tab geometry account for this layup not being entirely notch insensitive.

3. The failure mode for the $[0/90]_{2S}$ layup is transverse matrix cracking in the region of the hole, followed by longitudinal matrix splitting on the 0° plies and fiber breakage and pullout along the existing transverse cracks. Due to the initial transverse matrix cracks, the entire load is transferred to the 0° plies. The subsequent longitudinal splitting results in removal of the stress concentration, accounting for the notch insensitivity.

4. The Whitney-Nuismer (22) failure theory can be adapted to specimens of varying widths by expressing the equations in terms of the diameter

to width ratio instead of the radius. In this form, the Whitney-Nuismer theory fits the experimental data well. The Pipes *et al.* (16) modification to the Whitney-Nuismer theory can also be adapted to specimens of varying widths in the same manner. The Pipes *et al.* theory provides no improvement to the Whitney-Nuismer failure prediction for this material; however, it does provide a notch sensitivity parameter which quantifies relative notch sensitivity.

5. Acoustic emission techniques accurately indicate the point of initial damage in SiC/1723 ceramic matrix composites with holes (both $[0]_8$ and $[0/90]_{2S}$ layups). This is in agreement with previous work in unnotched ceramic matrix composites by Mall and Kim (13), Fink (9), and Bachmann (3), and is especially valuable when initial damage occurs in the region of a hole where it is difficult to observe. Strain gauges adjacent to the hole also provide reliable indication of initial damage.

6. In the $[0/90]_{2S}$ layup, this material sustains significant damage (sufficient to change the modulus) at a very low tensile stress, approximately 10-20% of ultimate. Bachmann (3) also noted transverse cracking of unnotched specimens of the same material at relatively low levels. This has important design implications for this material.

7. The measured axial modulus of elasticity for the $[0]_8$ layup is very close to the theoretically derived value; however, for the $[0/90]_{2S}$ layup it is approximately 80% of the theoretical value. This is not

unexpected, since the modulus of the $[0/90]_{2S}$ layup depends on the transverse modulus of the material. Transverse modulus is very sensitive to the quality of bond between fibers and matrix, while the theory assumes a perfect bond. There were also wide variations in the properties of the material from plate to plate.

Recommendations

While this study has increased the understanding of the performance of ceramic matrix composites with holes, there are several areas that deserve further consideration.

1. This study was performed entirely at room temperature, however, this material has been developed for high temperature use in gas turbine engines. Experiments should be conducted at high temperature on both notched and unnotched specimens.

2. It was found that beyond a certain stress level the load could be held fixed and strain would still increase, indicating continuing damage. It would be useful to determine if this material is load rate sensitive, i.e., if the failure stress is a function of the rate at which the load increases.

3. The specimens occasionally failed at the grips, due in part to the lack of control over the pressure applied to the specimens. A grip system should be used with which pressure can be measured and controlled directly. Also, compressive tests should be conducted on this material to determine the maximum stress that can be applied without inducing damage.

4. Additional tests should be conducted on the $[0]_8$ layup with tabs with

smaller tab angles. It is believed that a smaller tab angle contributed to a failure stress for one specimen of approximately 50% higher than expected.

Appendix: Sample Calculations

1. Effective Laminate Modulus

The calculation of modulus in the load direction (E_x) for the $[0/90]_{2S}$ layup is performed using the procedure discussed in Chapter II under Theoretical Background. This calculation need not be performed for the $[0]_8$ layup, since the lamina engineering properties can be used directly.

Using the properties for this material given in Chapter 4:

$$E_f = 164 \text{ GPa}$$

$$E_m = 60.6 \text{ GPa}$$

$$\nu_{12} = 0.18$$

and the volume fractions:

$$V_f = 0.45$$

$$V_m = 0.55$$

Equation (24): $E_1 = 164(0.45) + 60.6(0.55)$

$= 107.1$ GPa

Equation (25): $E2 = (164)(60.6)/[(0.55)(164)+(0.45)(60.6)]$

$= 84.6$ GPa

Equation (28): G12 = 164/[2(1+0.18)]

= 45.4 GPa

With these values the Aij extensional stiffness matrices can be computed as follows.

Equation (2) gives us the orthotropic plane stress compliance matrix:

$$[S] = \begin{bmatrix} 9.337 \times 10^{-3} & -1.681 \times 10^{-3} & 0 \\ -1.681 \times 10^{-3} & 1.182 \times 10^{-2} & 0 \\ 0 & 0 & 2.203 \times 10^{-2} \end{bmatrix} \text{GPa}^{-1}$$

and its inverse is the reduced stiffness matrix:

$$[Q] = [S]^{-1} = \begin{bmatrix} 109.9 & 15.6 & 0 \\ 15.6 & 86.8 & 0 \\ 0 & 0 & 45.4 \end{bmatrix} \text{GPa}$$

The transformation matrix for the 90° plies from Equation (4) is:

$$[T] = \begin{bmatrix} 0 & 1 & 0 \\ 1 & 0 & 0 \\ 0 & 0 & -1 \end{bmatrix}$$

Equation (5), with the [T] matrix above, gives $[\bar{Q}]$ for the 90° plies:

$$[\bar{Q}]_{90} = \begin{bmatrix} 86.8 & 15.6 & 0 \\ 15.6 & 109.9 & 0 \\ 0 & 0 & 45.4 \end{bmatrix} \text{ GPa}$$

For the 0° plies, $[\bar{Q}]$ is equal to [Q].

Using a nominal ply thickness of 0.3 mm (0.0003 m) and the relation for A_{ij} in Equation (6), the extensional stiffness matrix for the $[0]_8$ layup is:

$$[A] = \begin{bmatrix} 0.264 & 0.037 & 0 \\ 0.037 & 0.208 & 0 \\ 0 & 0 & 0.109 \end{bmatrix} \text{ GPa-meters}$$

and the extensional stiffness matrix for the $[0/90]_{2S}$ layup is:

$$[A] = \begin{bmatrix} 0.236 & 0.037 & 0 \\ 0.037 & 0.236 & 0 \\ 0 & 0 & 0.109 \end{bmatrix} \text{ GPa-meters}$$

The effective laminate modulus in the load direction for the $[0/90]_{2S}$ layup can now be calculated using the Aij matrix above. (As mentioned above, this is not necessary for the $[0]_8$ layup.) Equation (11), with a

nominal laminate thickness of 2.4 mm (0.0024 m), gives the result:

$$Ex = [(0.264)(0.208)-(0.037)^2]/[(0.208)(0.0024)]$$

$$= 95.9 \text{ GPa}$$

2. Whitney-Nuismer Failure Model

To calculate the Whitney-Nuismer failure stresses requires computation of Lekhnitskii's (12) stress concentration factor and Tan's (20) finite width correction factor. Equation (12) is the formula for the stress concentration in an infinite plate due to a circular hole; for the $[0]_8$ layup the result is:

$$K_T^{\infty} = 1 + \left\{ \frac{2}{0.208} \left[[(0.264)(0.208)]^{1/2} - 0.0375 + \frac{[(0.264)(0.208) - 0.0375^2]}{2(0.109)} \right] \right\}^{1/2}$$

$$= 3.06$$

The Tan finite width correction factor, Equation (13), for a D/W ratio of 0.27 in the $[0]_8$ layup is:

$$\frac{K_T^{\infty}}{K_T} = \frac{3(1 - 0.27)}{2 + (1 - 0.27)^3} + \frac{1}{2}(0.27M)^6 (3.06 - 3)[1 - (0.27M)^2]$$

where M for this example, by Equation (14), is:

$$M^2 = \frac{\left\{1 - 8\left(\frac{3(1 - 0.27)}{2 + (1 - 0.27)^3} - 1\right)\right\}^{1/2} - 1}{2(0.27)^2}$$

resulting in:

$$\frac{K_T^{\infty}}{K_T} = 1.0882$$

The same procedure is followed for other D/W ratios and for the other layup.

To apply the Whitney-Nuismer point stress criterion, Equation (17) is replaced with Equation (29). The optimum value for $(D/W)_{do}$ is found by least-squares error minimization to be 0.084 for the $[0]_8$ layup, so for the example of a specimen with D/W = 0.27, Equation (29) yields:

$$\xi_1 = \frac{0.27}{0.27 + 0.084}$$

$$= 0.763$$

which is used in Equation (16):

$$\frac{\sigma_N^{\infty}}{\sigma_o} = \frac{2}{2 + (0.763)^2 + 3(0.763)^4 - (3.06 - 3)[5(0.763)^6 - 7(0.763)^8]}$$

$$= 0.558$$

For the average stress criterion, Equation (19) is replaced with Equation (30). The optimum value for $(D/W)_{ao}$ is found by least-squares error minimization to be 0.232 for the $[0]_8$ layup, so for the example of a specimen with D/W = 0.27, Equation (30) yields:.538

$$\xi_2 = \frac{0.27}{0.27 + 0.232}$$

$$= 0.538$$

which is then used in Equation (18):

$$\frac{\sigma_N^\infty}{\sigma_\bullet} = \frac{2(1 - 0.538)}{2 - (0.538)^2 - (0.538)^4 + (3.06 - 3)[(0.538)^6 - (0.538)^8]}$$

$$= 0.568$$

As before, the same procedure is followed for other D/W ratios and for the $[0/90]_{2S}$ layup.

3. Pipes et al. Failure Model

The Pipes et al. modification to the Whitney-Nuismer model, Equation (23) is replaced by Equation (32). It is found by iterative error minimization that the best value of m is 0 for this material in both

layups, and the optimum value of C (the notch-sensitivity parameter) is 11.9 cm^{-1} for the $[0]_8$ layup. Continuing the example of a D/W ratio = 0.27, Equation (32) gives:

$$\lambda = [1 + (0.27)^{-1}(11.9)^{-1}]^{-1}$$

$$= 0.763$$

which is the same value as obtained for ξ_1 in the Whitney-Nuismer example above. This is then used to solve Equation (22), but the equation reverts to the Whitney-Nuismer relation, so it is not shown here.

Bibliography

1. Awerbuch, Jonathan and Shahrokh Ghaffari. "Tracking Progression of Matrix Splitting During Static Loading Through Acoustic Emission in Notched Unidirectional Graphite/Epoxy Composites," *ANTEC 1987*: 1069-1074

2. Awerbuch, J.A., and M.S. Madhukar, "Notched Strength of Composite Laminates, Predictions and Experiments—A Review," *Journal of Reinforced Plastics and Composites, 4*: 3-159 (January 1985)

3. Bachmann, Capt Steven E. *Transverse Cracking In A Fiber Reinforced Ceramic Matrix Composite*. MS Thesis, AFIT/GAE/ENY/90D-2. School of Engineering, Air Force Institute of Technology (AU), Wright-Patterson AFB OH, December 1990

4. Brennan, J.J. and K.M. Prewo, " Silicon Carbide Fibre Reinforced Glass-Ceramic Matrix Composites Exhibiting High Strength and Toughness," *Journal of Materials Science, 17*: 2371-2383 (August 1982)

5. Chang, Kuo-Yen *et al.* "Damage Tolerance of Laminated Composites Containing an Open Hole and Subjected to Tensile Loadings," *Journal of Composite Materials, 25*: 274-301 (March 1991)

6. Cunningham, Mary E. *et al.* "Effect of End-Tab Design on Tension Specimen Stress Concentrations," *Recent Advances in Composites in the United States and Japan, ASTM STP 864,* edited by J.R. Vinson and M. Taya. Philadelphia, American Society for Testing and Materials, 1985

7. Dunegan, H.L. *et al.* "Fracture Analysis by Use of Acoustic Emission," *Engineering Fracture Mechanics, 1*: 105-122 (January 1968)

8. Evans, A.G. "The Mechanical Performance of Fiber-Reinforced Ceramic Matrix Composites," *Materials Science and Engineering, A107*: 227-239 (1989)

9. Fink, Capt Walter E. *Investigation of Failure Modes In A Ceramic Composite Under Off-Axis Loading.* MS Thesis, AFIT/GAE/ENY/89D-9. School of Engineering, Air Force Institute of Technology (AU), Wright-Patterson AFB OH, December 1989

10. Greszczuk, L.B. "Stress Concentrations and Failure Criteria for Orthotropic and Anisotropic Plates with Circular Openings," *Composite Materials: Testing and Design (Second Conference), ASTM STP 497,* Philadelphia, American Society for Testing and Materials, 1972

11. Jones, Robert M. *Mechanics of Composite Materials.* New York: Hemisphere Publishing Corporation, 1975

12. Lekhnitskii, S.G. *Anisotropic Plates.* Translated from the Second Russian Edition by S.W. Tsai and T. Cheron. New York, Gordon and Breach Science Publishers, 1968

13 Mall,S. and R. Y. Kim, "Damage Initiation and Growth in a Quasi-Isotropic Laminate of Ceramic Matrix Composite," *Proceedings of the 1990 SEM Spring Conference on Experimental Mechanics,* Albuquerque, New Mexico: 732-737 (June 1990)

14. Marshall, D.B. and A.G. Evans, "Failure Mechanisms in Ceramic-Fiber/Ceramic Matrix Composites," *Journal of the American Ceramic Society, 68*: 225-231 (May 1985)

15. Moschelle, Capt William. *Fatigue Behavior and Failure Mechanisms of Centrally Notched $[0]_8$ and $[0/90_2]_S$ Silicon Carbide Reinforced Aluminosilicate Glass,* MS Thesis, AFIT/GAE/ENY/91D-19, School of Engineering, Air Force Institute of Technology (AU), Wright-Patterson AFB OH, December 1991

16. Pipes et al. "Notched Strength of Composite Materials," *Journal of Composite Materials, 12*: 148-160 (1974)

17. Prewo, K.M. and J.J. Brennan, "Silicon Carbide Yarn Reinforced Glass Matrix Composites," *Journal of Materials Science, 17*: 1201-1206 (April 1982)

18. Tan, Seng C. "Mixed-Mode Fracture of Notched Unidirectional and Off-Axis Laminates under Tensile Loading," *Journal of Composite Materials, 23*: 1082-1105 (November 1989)

19. Tan, S.C. "Notched Strength Prediction and Design of Laminated Composites Under In-Plane Loadings," *Journal of Composite Materials, 21*: 750-779 (August 1987)

20. Tan, Seng C. "Finite-Width Correction Factors for Anisotropic Plate Containing a Central Opening," *Journal of Composite Materials, 22*: 1080-1097 (November 1988)

21. Weng, T. *et al*. "Damage analysis in Reinforced LCP Composites by Acoustic Emission Location Techniques," *Journal of Composite Materials, 24*: 103-121 (January 1990)

22. Whitney, J.M. and R.J Nuismer. "Stress Fracture Criteria for Laminated Composites Containing Stress Concentrations," *Journal of Composite Materials, 8*: 253-265 (July 1974)

23. Zawada, L.P., ceramics engineer, Metals and Ceramics Division, Air Force Materials Laboratory. Personal interviews. WL/MLLN, Wright-Patterson AFB OH, October-November 1991.

REPORT DOCUMENTATION PAGE

Form Approved
OMB No 0704-0188

1. AGENCY USE ONLY (Leave blank)	2. REPORT DATE	3. REPORT TYPE AND DATES COVERED
	December 1991	Master's Thesis

4. TITLE AND SUBTITLE
Failure Characterization of a Fiber Reinforced Ceramic Matrix Composite With Circular Holes

5. FUNDING NUMBERS

6. AUTHOR(S)
Daniel E. Bullock, Captain, USAF

7. PERFORMING ORGANIZATION NAME(S) AND ADDRESS(ES)
Air Force Institute of Technology, WPAFB OH 45433-6583

8. PERFORMING ORGANIZATION REPORT NUMBER
AFIT/GAE/ENY/91D-20

9. SPONSORING / MONITORING AGENCY NAME(S) AND ADDRESS(ES)
Captain John Pernot
WL/MLLN
Wright-Patterson AFB OH 45433

10. SPONSORING / MONITORING AGENCY REPORT NUMBER

11. SUPPLEMENTARY NOTES

12a. DISTRIBUTION / AVAILABILITY STATEMENT
Approved for public release; distribution unlimited

12b. DISTRIBUTION CODE

13. ABSTRACT (Maximum 200 words)

The purpose of this study was to investigate the performance of a fiber reinforced ceramic matrix composite (SiC/1723) with central circular holes. Objectives were to determine the relationship between tensile failure stress and the ratio of hole diameter to specimen width, and to examine the initiation and progression of damage. Unidirectional and cross-ply layups were tested at room temperature. Damage data were gathered using acoustic emission, strain gauges, replication techniques, and ultrasound (C-scan). The Whitney-Nuismer failure theory was adapted to allow for specimens of varying widths, and was found to fit the experimental data well.

The failure mode for the symmetric layup was longitudinal matrix splitting, initiating at the edge of the hole. In the cross-ply layup, the failure mode was transverse matrix cracking in the region of the hole followed by longitudunal matrix cracking in the 0 degree plies and fiber breakage along the existing transverse cracks. The failure modes for both layups followed the same pattern as graphite epoxy composites.

It was determined that this material is largely insensitive to holes in both layups; in the cross-ply layup, the ultimate load can be predicted directly from the notched section area.

14. SUBJECT TERMS	15. NUMBER OF PAGES
Composites, composite materials, ceramics, brittle matrix, ceramic matrix, holes	121
	16. PRICE CODE

17. SECURITY CLASSIFICATION OF REPORT	18. SECURITY CLASSIFICATION OF THIS PAGE	19. SECURITY CLASSIFICATION OF ABSTRACT	20. LIMITATION OF ABSTRACT
Unclassified	Unclassified	Unclassified	UL